# Spin-Lattice Relaxation in Some Rare-Earth Salts. I. Temperature Dependence*

G. H. LARSON AND C. D. JEFFRIES
*Physics Department, University of California, Berkeley, California*
(Received 11 August 1965)

We report measurements of the spin-lattice relaxation rate $T_1^{-1}$ for several magnetically dilute rare-earth ions in the temperature range $1.2°\leqq T\leqq 5°$K, using the transient recovery of the microwave paramagnetic resonance in the frequency range $8\leqq\nu\leqq 18$Gc/sec. Data are given for $Sm^{3+}$ and $Dy^{3+}$ in the double nitrate $La_2Mg_3(NO_3)_{12}\cdot 24H_2O$; for $Pr^{3+}$, $Sm^{3+}$, and $Er^{3+}$ in the ethyl sulfate $La(C_2H_5SO_4)_3\cdot 9H_2O$; and for $Ce^{3+}$, $Nd^{3+}$, $Pr^{3+}$, $Sm^{3+}$, $Er^{3+}$, and $Tb^{3+}$ in the ethyl sulfate $Y(C_2H_5SO_4)_3\cdot 9H_2O$. We observe the temperature dependence for the direct process $T_1^{-1}\propto T$; for the Orbach process $T_1^{-1}\propto \exp(-\Delta/T)$; and for the Raman process $T_1^{-1}\propto T^7$ or $T^9$. The magnitudes of the processes are in reasonable agreement with simple theoretical estimates. The observed rates are shown to be independent of paramagnetic ion concentration in the range 0.1 to 1%. For Pr in the ethyl sulfate, we observe, as expected, a phonon bottleneck rate $T_b^{-1}\propto T^2$ rather than the direct process. In several cases the Orbach process determines a previously unknown value of the crystal-field splitting $\Delta$, while in some cases it shows that the value of $\Delta$ in the dilute salt is significantly different from the value determined optically in the concentrated salt.

## I. INTRODUCTION

DURING the last few years many experiments have been reported[1–10] on paramagnetic relaxation of rare-earth ions at low temperature, especially for ions diluted in diamagnetic host crystals, where a particularly useful method is to observe the transient recovery of the microwave paramagnetic-resonance absorption following a saturating pulse. The older classical theories[11–14] have been reexamined and put into a phenomenological form by Orbach,[15] which facilitates the calculation of theoretical estimates; in general, reasonable agreement is found with the experimental results.

In this paper we report on some further measurements and theoretical calculations on a number of rare-earth ions in the host crystals: lanthanum magnesium double nitrate $La_2Mg_3(NO_3)_{12}\cdot 24H_2O$ ["LaMN"]; lanthanum ethyl sulfate $La(C_2H_5SO_4)_3\cdot 9H_2O$ ["LaES"]; and yttrium ethyl sulfate $Y(C_2H_5SO_4)_3\cdot 9H_2O$ ["YES"]. Basically this paper is an extension of the work of Scott and Jeffries[2] (S&J), to which we refer for fuller details. Here we are primarily concerned with the temperature dependence of the various relaxation processes in the liquid-helium range. In a later paper we will discuss the dependence on magnetic field and orientation of the crystals, as well as cross relaxation effects.

After a brief review of the theory in Sec. II, we describe the apparatus and the crystals in Sec. III. In Sec. IV are presented the data and the theoretical estimates for a number of cases.

## II. REVIEW OF THEORY

For a magnetically dilute single crystal in a magnetic field $H$ and immersed in a liquid-helium bath at temperature $T$ we take for the static Hamiltonian of the electronic ground state

$$\mathcal{H}=\mathcal{H}_{so}+\mathcal{H}_c+\mathcal{H}_Z,\ \cdots \tag{1}$$

the terms representing the spin-orbit, crystal-field, and Zeeman interactions. To fix ideas we consider the $Ce^{3+}$ ion with a ground state $4f^1\,{}^2F_{5/2}$, as in Fig. 1. The spin-orbit interaction places the next multiplet, ${}^2F_{7/2}$, higher by 2240 $cm^{-1}$. The crystal field in YES splits the ground multiplet into three levels, the spacing between the lowest two being $\Delta_1\approx 17.4$ $cm^{-1}$. The magnetic field further splits these into Kramers doublets $|a\rangle$ and $|b\rangle$, $|c\rangle$ and $|d\rangle$, and $|e\rangle$ and $|f\rangle$; each are characterized to a good approximation by a linear combination of the basic spin functions $|J,J_z\rangle$, where $J=\frac{5}{2}$ is a good quantum number. The Zeeman splitting is usually given, e.g., for $z\|H$, by

$$h\nu=\delta=2|\langle a|\Lambda\beta HJ_z|a\rangle|\,, \tag{2}$$

where $\Lambda$ is the Landé $g$ factor and $\beta$ is the Bohr magneton.

The basic problem of relaxation theory is to calculate the transition rates between these levels due to the lattice vibrations. It is now well established that the Van Vleck-Kronig-Fierz[13,14,15a] mechanism of thermal

* Research supported in part by the U. S. Atomic Energy Commission and the Office of Naval Research.

[1] C. B P. Finn, R. Orbach, and W. P. Wolf, Proc. Phys. Soc. (London) **77**, 261 (1961).
[2] P. L. Scott and C. D. Jeffries, Phys. Rev. **127**, 32 (1962).
[3] R. H. Ruby, H. Benoit, and C. D. Jeffries, Phys. Rev. **127**, 51 (1962).
[4] J. A. Cowen, D. E. Kaplan, and M. E. Browne, J. Phys. Soc. Japan **17**, Suppl. B-I, 465 (1962).
[5] J. Van den Broek and L. C. Van der Marel, Physica **29**, 948 (1963); **30**, 565 (1964).
[6] I. Svare and G. Seidel, in *Paramagnetic Resonance*, Proceedings of the First International Conference, Jerusalem, 1962, edited by W. Low (Academic Press Inc., New York, 1963), Vol. II, p. 430.
[7] J. M. Baker and N. Ford, Phys. Rev. **136**, A1692 (1964).
[8] M. Schulz and C. D. Jeffries, Bull. Am. Phys. Soc. **9**, 739 (1964).
[9] G. H. Larson and C. D. Jeffries, Bull. Am. Phys. Soc. **9**, 739 (1964).
[10] C. Y. Huang, Phys. Rev. **139**, A241 (1965).
[11] I. Waller, Z. Physik **79**, 370 (1932).
[12] W. Heitler and E. Teller, Proc. Roy. Soc. (London) **155**, 629 (1936).
[13] J. H. Van Vleck, Phys. Rev. **57**, 426 (1940).
[14] R. de L. Kronig, Physica **6**, 33 (1939).
[15] R. Orbach, Proc. Roy. Soc. (London) **A264**, 458 (1961).
[15a] M. Fierz, Physica **5**, 433 (1938).

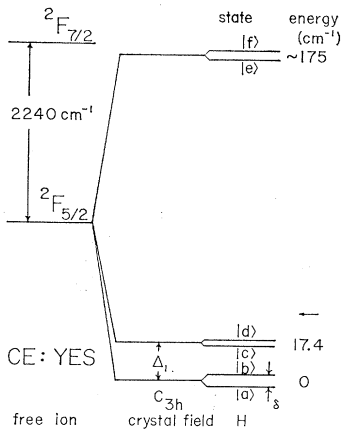


FIG. 1. Splitting of the $^2F_{5/2}$ ground state of magnetically dilute $Ce^{3+}$ in YES. The value of $\Delta_1/hc = 17.4$ cm$^{-1}$ is taken from the observed Orbach relaxation term. The arrow in the energy column on this diagram and any that follow means that energy values above the arrow are calculated while those below are experimental; otherwise the values are all experimental numbers. Paramagnetic resonance and relaxation are observed between the ground doublet $|a\rangle$, $|b\rangle$ where $\delta = h\nu$.

modulation of the crystalline electric fields is dominant over the Waller mechanism of modulation of magnetic dipolar coupling between paramagnetic ions. Although a proper approach is through the normal modes of the vibrating charge complex surrounding the ion,[13] the low-point symmetry of the rare-earth site in our crystals and the fact that $J$ is a good quantum number leads to a simple phenomenological approach introduced by Orbach,[15] based on the static-crystal-field theory for these salts,[16–21] wherein one writes an expansion

$$\mathcal{H}_c = \sum_{nm} V_n^m = \sum_{\substack{n=2,4,6 \\ -n \leqq m \leqq n}} A_n^m G_n^m(x,y,z), \qquad (3)$$

where the $G_n^m$ are unnormalized Legendre polynomials. The matrix elements of the expectation value of $\mathcal{H}_c$ over the $f$ electrons of the ion can be evaluated using the operator equivalent method:

$$\langle a|\mathcal{H}_c|b\rangle = \sum_{nm} A_n^m \langle r^n\rangle \chi_n \langle a|o_n^m|b\rangle, \qquad (4)$$

where $\chi_n$ are operator equivalent factors, equal to the $\alpha$, $\beta$, and $\gamma$ of Stevens[16] for $n=2$, 4, and 6, respectively. The $o_n^m$ are operators in $J_z$ and $J_\pm$, defined by $o_n^{+m} + o_n^{-m} = O_n^m$, where the $O_n^m$ are operators listed by Orbach.[15] Tables of matrix elements are available.[22]

The important point here is that for the well-known crystals we have used, the values of the crystal-field parameters $A_n^m\langle r^n\rangle$ and the wave functions $|a\rangle$, $|b\rangle$, $\cdots$ have in many cases been determined by optical spectroscopic and paramagnetic resonance data. For example, Fig. 2 shows the values of $A_2^0\langle r^2\rangle$, $A_4^0\langle r^4\rangle$, $A_6^0\langle r^6\rangle$, and $A_6^6\langle r^6\rangle$, the only nonvanishing terms for the rare-earth ethyl sulfates, which have $C_{3h}$ point symmetry about the rare-earth site; the data are mainly taken from Hüfner's review[23] for the magnetically concentrated salts, but the parameters for ions diluted in LaES and YES are known to be similar except in cases noted below. By analogy to Eqs. (3) and (4), it is reasonable to assume that the average thermal lattice strain $\epsilon$ produces a deformation given approximately by

$$\mathcal{H}_c' = \epsilon \sum_{nm} v_n^m, \qquad (5)$$

which acts as a random time-dependent perturbation to induce relaxation transitions between the states of Fig. 1, with a typical matrix element

$$\langle a|\mathcal{H}_c'|b\rangle = \epsilon \sum_{nm} a_n^m \langle r^n\rangle \chi_n \langle a|o_n^m|b\rangle. \qquad (6)$$

The dynamic-crystal-field parameters $a_n^m$ may be expected to have the approximate magnitude of the static parameters $A_n^m$; however, the deformation may have such low symmetry that all the $a_n^m$ are nonvanishing, so that a scheme for estimating the many $a_n^m$ from the few measured values $|A_n^m|_{\text{exp}}$ is necessary. At least two approximations have been used. For the double

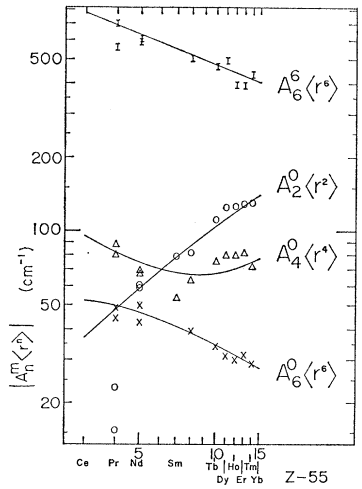


FIG. 2. Optically measured values of the crystal field parameters $|A_n^m\langle r^n\rangle|$ for the concentrated ethyl sulfates $X(C_2H_5SO_4)_3 \cdot 9H_2O$. This diagram is taken from Hüfner (Ref. 23) with additional data added for $Nd^{3+}$ (Ref. 36) and $Pr^{3+}$ (Ref. 33).

[16] K. W. H. Stevens, Proc. Phys. Soc. (London) **A65**, 209 (1952).
[17] R. J. Elliott and K. W. H. Stevens, Proc. Roy. Soc. (London) **A215**, 437 (1952).
[18] R. J. Elliott and K. W. H. Stevens, Proc. Roy. Soc. (London) **A218**, 553 (1953).
[19] R. J. Elliott and K. W. H. Stevens, Proc. Roy. Soc. (London) **A219**, 387 (1953).
[20] B. R. Judd, Proc. Roy. Soc (London) **A227**, 552 (1955).
[21] B. R. Judd, Proc. Roy. Soc. (London) **A232**, 458 (1955).
[22] H. A. Buckmaster, Can. J. Phys. **40**, 1670 (1962); R. C. Mikkelson and H. J. Stapleton, report by Dept. of Physics and Materials Research Laboratory, University of Illinois, Urbana, Illinois, 1964 (unpublished); M. T. Hutchings, Solid State Phys. **16**, 227 (1965).
[23] S. Hüfner, Z. Physik **169**, 417 (1962).

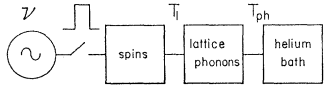


FIG. 3. Schematic thermal block diagram of the microwave oscillator, paramagnetic spin system, lattice phonon system, and the helium bath.

nitrates, the dominating crystal field is icosahedral,[24] with a weaker $C_{3v}$ symmetry component, yielding the empirical rule that $|B_n^m| \approx |B_n^0|$ in a normalized spherical harmonic expansion $B_n^m r^n Y_n^m$ of $\mathcal{H}_c$. Thus S&J arrive at the approximation

$$|a_n^m| = g_n^{|m|} |A_n^0|_{\exp}, \quad n=2,4,6, \tag{7}$$

with the factors $g_n^{|m|}$ given in Table I. For the ethyl sulfates Orbach has suggested

$$g_n^{|m|} = 1, \quad n=2,4, \tag{8a}$$

$$|a_6^m| = [|A_6^0|_{\exp}{}^{6-|m|} |A_6^6|_{\exp}{}^{|m|}]^{1/6}. \tag{8b}$$

Equations (8a) and (8b) yield dynamic terms most of which are two to ten times smaller than those estimated using Eq. (7). Anticipating our results, we note that in cases where the $a_6^n$ occur (that is, when $J \geqq 3$) they usually dominate the calculations and scheme Eq. (7) gives better agreement with experiment. However, in the ethyl sulfates, the four cases where $J=\frac{5}{2}$ ($Sm^{3+}$ and $Ce^{3+}$ in both LaES and YES) are better explained using scheme Eq. (8a).

In calculating relaxation rates one requires the square of the magnitude of the matrix element of Eq. (6), which raises the question of the coherence of the various terms. S&J conclude that the best approximation is to assume each term $o_2^0$, $o_2^{+1}$, $o_2^{-1}$, $\cdots$ incoherent. We explicitly take

$$|\langle a|\sum_{nm} v_n^m|b\rangle|^2 = \sum_{nm} |\langle a|v_n^m|b\rangle|^2 = \sum_{\substack{n=2,4,6 \\ -n\leqq m\leqq n}} |\chi_n g_n^{|m|} |A_n^0\langle r^n\rangle|_{\exp} \langle a|o_n^m|b\rangle|^2, \tag{9}$$

where the $|A_n^0\langle r^n\rangle|_{\exp}$ are measured in ergs.

Our experiments are performed in the $He^4$ temperature range, where usually only the lowest doublet $|a\rangle$, $|b\rangle$ is appreciably populated. We monitor the population difference $\eta = N_a - N_b$ by microwave paramagnetic resonance at frequency $\nu = \delta/h$, and measure the transient return to thermal equilibrium after the spin temperature has been raised to infinity by a saturating microwave pulse. The recovery is usually found to be exponential, with the observed time constant denoted by $T_b$, the "spin-bath" relaxation time. The schematic thermal block diagram of Fig. 3 indicates the arrangement: after the pulse the spins relax to the lattice phonons at the rate $T_1^{-1}$ sec$^{-1}$; the phonons relax to the helium bath at the rate $T_{\rm ph}^{-1}$ sec$^{-1}$. If $\sigma \equiv (C_s/C_p) \times (T_{\rm ph}/T_1) \ll 1$, where $C_s/C_p$ is the specific-heat ratio of spins to phonons, then the phonon temperature is maintained at the helium-bath temperature $T$; the observed time constant $T_b$ is thus expected to be $T_1$. On the other hand, if $\sigma \gg 1$, the phonons cannot transport the excess spin energy to the bath rapidly enough, and a phonon bottleneck develops. In this case, the observed time constant becomes $T_b \approx T_{\rm ph}(C_s/C_p)$, as discussed in detail by S&J: the experiment yields the phonon-bath relaxation time $T_{\rm ph}$ rather than the spin-lattice relaxation time. More explicitly, the observed relaxation rate is expected to be

$$\frac{1}{T_b} = \frac{12\pi\nu^2\Delta\nu}{T_{\rm ph} v^3 c}\left[\coth\left(\frac{h\nu}{2kT}\right)\right]^2 \approx DT^2, \tag{10a}$$

where $\Delta\nu$ is the EPR linewidth, $v$ is the velocity of sound, and $c$ is the number of paramagnetic ions per $cm^3$.

At the lowest temperatures the dominant contribution to the spin-lattice relaxation rate $T_1^{-1}$ is the direct process, in which the spin flips give their energy to phonons of the frequency $\nu$, yielding a relaxation rate [S&J, Eq. (17)]

$$\frac{1}{T_{1d}} = \frac{3}{2\pi\rho v^5 \hbar}\left(\frac{\delta}{\hbar}\right)^3 \sum_{nm} |\langle a|v_n^m|b\rangle|^2 \coth\left(\frac{\delta}{2kT}\right), \tag{10b}$$

where $\rho$ is the crystal density and $v$ is the velocity of sound. For most of our work $\coth(\delta/2kT) \approx 2kT/\delta$, and so Eq. (10b) can be rewritten as

$$1/T_{1d} = AT. \tag{10c}$$

The condition that the direct process not be bottlenecked is $DT^2 \gg AT$ in Eqs. (10a) and (10c). Although Eq. (10b) is suitable for a non-Kramers doublet $|a\rangle$, $|b\rangle$, it vanishes in zero order for Kramers doublets; one must then take account of admixtures into $|a\rangle$ and $|b\rangle$ of the higher states through the Zeeman perturbation $\mathcal{H}_Z$. The result is

$$\frac{1}{T_{1d}} = \frac{3}{2\pi\rho v^5 \hbar}\left(\frac{\delta}{\hbar}\right)^3 \sum_{nm} \left| \sum_i \left(\frac{2\beta\Lambda}{\Delta_i}\right) (\langle a|\mathbf{H}\cdot\mathbf{J}|i\rangle\langle i|v_n^m|b\rangle + \langle a|v_n^m|i\rangle\langle i|\mathbf{H}\cdot\mathbf{J}|b\rangle) \right|^2 \left(\frac{2kT}{\delta}\right) \equiv A'T, \tag{11}$$

where $|i\rangle$ is one of the states for each higher Kramers

TABLE I. Values of the normalizing factors $g_n^{|m|}$ used in Eq. (7).

| $\|m\|=$ | 1 | 2 | 3 | 4 | 5 | 6 |
|---|---|---|---|---|---|---|
| $n=2$ | 4.90 | 2.45 | | | | |
| $n=4$ | 8.95 | 6.32 | 23.6 | 8.37 | | |
| $n=6$ | 12.9 | 10.2 | 20.2 | 11.2 | 52.7 | 15.2 |

[24] B. R. Judd, Proc. Roy. Soc. (London) **A241**, 122 (1957); B. R. Judd and E. Y. Wong, J. Chem. Phys. **28**, 1097 (1958); A. G. McLellan, *ibid.* **34**, 1350 (1961).

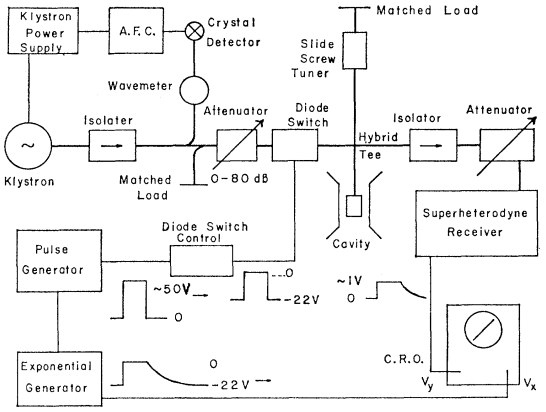


FIG. 4. Block diagram of the bridge spectrometer used for measuring relaxation times at $\nu \approx 9.3$ Gc/sec.

doublet. For axial crystals we take $\mathbf{H}\cdot\mathbf{J}=H(J_z\cos\theta+J_x\sin\theta)$.

If the crystal field splitting $\Delta_1$ is less than the Debye energy $k\Theta$ ($\Theta\approx 60°$K for our crystals), then relaxation between $|a\rangle$ and $|b\rangle$ may proceed through a two-step Orbach process involving a transition from $|b\rangle$ up to an excited state $|c\rangle$, and then back down to $|a\rangle$; the resulting relaxation rate is

$$\frac{1}{T_{10}}=\frac{3}{2\pi\rho v^5\hbar}\left(\frac{\Delta_1}{\hbar}\right)^3 \times\frac{2\sum_{nm}|\langle a|v_n{}^m|c\rangle|^2\sum_{nm}|\langle c|v_n{}^m|b\rangle|^2}{(\sum_{nm}|\langle a|v_n{}^m|c\rangle|^2+\sum_{nm}|\langle c|v_n{}^m|b\rangle|^2)} \times\frac{1}{\exp(\Delta_1/kT)-1} \quad (12a)$$

In most cases $\exp(\Delta_1/kT)-1\approx\exp(\Delta_1/kT)$, and Eq. (12a) can be approximately written as

$$1/T_{10}=B\exp(-\Delta_1/kT). \quad (12b)$$

If instead of an excited singlet $|c\rangle$ we have a Kramers doublet $|c\rangle$ and $|d\rangle$, a term for $|d\rangle$ must be added to Eq. (12a) similar to that for $|c\rangle$. The two terms are in fact equal, so that for an excited doublet we need only multiply Eq. (12a) by a factor of 2.

The higher order Raman process involves the simultaneous absorption of a phonon of energy $\delta_1$, and the emission of another of energy $\delta_2=\delta_1+\delta$, along with a spin flip from $|b\rangle$ to $|a\rangle$. The relaxation rates due to this process are approximately [cf. S&J Eqs. (27) and (28b)]

$$\frac{1}{T_{1R}}=\frac{9\times 6!}{4\rho^2\pi^3 v^{10}}\left(\frac{k}{\hbar}\right)^7\left[\sum_{nm}|\langle a|v_n{}^m|b\rangle|^2+\sum_i\frac{1}{\Delta_i{}^2}\times\{\sum_{nm}|\langle a|v_n{}^m|j\rangle|^2\sum_{nm}|\langle j|v_n{}^m|b\rangle|^2\}\right]T^7\equiv cT^7, \quad (13)$$

for a non-Kramers doublet, where $j$ is a higher state. For a Kramers salt

$$\frac{1}{T_{1R}}=\frac{9!\hbar^2}{\pi^3\rho^2 v^{10}}\left(\frac{k}{\hbar}\right)^9\sum_i\frac{1}{\Delta_i{}^4}\sum_{nm}|\langle a|v_n{}^m|i\rangle|^2 \times\sum_{nm}|\langle i|v_n{}^m|b\rangle|^2T^9\equiv c'T^9, \quad (14)$$

where $|i\rangle$ is one of the states for each higher doublet.

To summarize, we assume that all the processes add to give a total spin-lattice relaxation rate for a ground state doublet $T_1{}^{-1}=T_{1d}{}^{-1}+T_{10}{}^{-1}+T_{1R}{}^{-1}$.

For evaluating the matrix elements and the sum of their squares in the above expressions we have used an IBM 7094 computer with a program based on one written by Mikkelson and Stapleton.[25]

## III. APPARATUS AND TECHNIQUES

The spin-bath relaxation time $T_b$ was measured by the method described in detail in S&J, in which the recovery of the microwave paramagnetic resonance is monitored at a very low power level, following a saturating microwave pulse of duration $\tau$. Several different microwave spectrometers were used: the transmission type shown in S&J Fig. 2 operating at a fixed frequency of $\nu=9.3$ Gc/sec; and a bridge-type spectrometer, with a tunable cavity, shown in Figs. 4 and 5. Varian X-13 and X-12 klystrons provided cw power in the range 8.2–18 Gc/sec; an automatic frequency control (AFC) circuit was used to lock the klystron to the frequency of a cavity wave meter. A wave guide switch with an off-on ratio between 20 and 50 dB was used to provide the saturating pulse. Two switches were used in the 8.2–12 Gc/sec range: the one described in S&J; and a Philco switch mount P901A with L4146 or L4136 germanium diodes. In the 12–18 Gc/sec range the

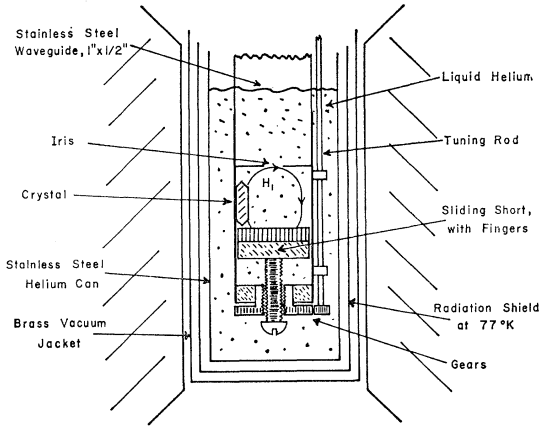


FIG. 5. Diagram of the tunable, rectangular $TE_{101}$ cavity in the tip of the Dewar between the pole faces of the magnet, which produces $H=19$ kOe in a 2 in. gap.

[25] R. C. Mikkelson and H. J. Stapleton (private communication).

following arrangement was used: the S&J switch was mounted in one side arm of a hybrid tee, the other arm being connected to a slide screw tuner and a variable shorting plunger. It was possible to then balance for an off-on transmission ratio of 20–30 dB between the $E$ and $H$ arms.

The transient recovery of the signal from the superheterodyne receiver (type APS/19) was observed with an oscilloscope, photographed, and replotted on a semilog graph to determine if the decay was exponential, and to obtain the time constant $T_b$. After an initial rapid nonexponential recovery due to amplifier overloading and possible cross relaxation within the linewidth, the signals were generally exponential in the tails, and did not depend on the pulse length or pulse power except as noted below. Because of the large amount of data involved in this work we often used a direct electronic method of observing the recovery, as shown in Fig. 4: at the end of the saturating microwave pulse an exponential generator is triggered to produce a voltage $V_x=-V_0[1-\exp(-t/\tau')]$, where $\tau'$ is adjustable by a calibrated $RC$ network. The signal voltage from the superheterodyne receiver is given by $V_y=V_0\exp(-t/T_b)$, so that a straight line $V_y=V_x+V_0$ of slope 45° appears on the scope if $\tau'$ is adjusted to the value $T_b$. Besides being much faster than the photographic method, this technique has higher accuracy and reproducibility ($\pm 5\%$) because it involves a visual integration of several seconds, which increases the signal-to-noise ratio over that of a single photograph. The raw data were first plotted $T_b^{-1}$ versus $T$ on log-log paper, to see if terms $AT$ and $CT^9$ could be recognized; then $T_b^{-1}$-$AT$-$CT^9$ versus $T^{-1}$ was replotted on semilog paper to determine any Orbach term of the form $B\exp(-\Delta/kT)$. In the later experiments a least square computer program was used to fit the raw data.

The crystals were always immersed in the liquid helium which filled the cavity; data were taken over the range $1.2<T<5$°K by pumping or pressurizing the helium; the pressure was stabilized with a Cartesian manostat; the temperature was obtained from the $He^4$ vapor pressure.

The crystals were grown in a dessicator at 0°C from a saturated aqueous solution of LaMN, LaES, or YES containing a small fraction of the paramagnetic rare-earth ion X under investigation. The concentrations of X quoted in Sec. IV refer to the relative concentration in the growing solution, which is probably close to that in the crystal, except in cases noted below, where the paramagnetic ion is highly rejected. The growing solutions were prepared from 99.997% La, 99.9999% Y, and 99.9% X, all obtained from Lindsay Chemical Corporation. The magnesium nitrate was Mallinckrodt Analytical Reagent, containing less than 0.0005% Fe. The ethyl sulfates were prepared from barium ethyl sulfate, City Chemical Corporation, Electronic Grade, with Fe impurities less than 6 ppm, Cr impurities $<18$ ppm. The procedure of Erath[26] was used in synthesizing the rare-earth ethyl sulfates.

The rhombohedral crystal structure of CeMN is well known[27]; it is isostructural with LaMN; there is only one rare-earth site, surrounded by 12 oxygen atoms (belonging to 6 nitrate ions) at the corners of a somewhat irregular icosahedron. The La-La spacing is approximately 8.5 Å. The crystals grow in flat hexagonal plates with the $z$ axis of the $g$ tensor perpendicular to the plate. Our crystals were typically 1.5 mm thick and 6 mm in diameter.

The ethyl sulfates LaES and YES are presumably isostructural,[28] but the crystal-field parameters and the $g$ factors are occasionally noticeably different, as mentioned in Sec. IV. We often used YES rather than LaES because the available purity is an order of magnitude higher. There is a single rare-earth site of $C_{3h}$ point symmetry, with two nearest rare-earth neighbors at $\sim 7$Å along the $z$ axis, and 6 next-nearest at $\sim 9$ Å. Since the $z$ axis is not always recognizable by visual inspection we oriented the samples by use of x rays. There is some evidence for Dy and Yb in LaES that there are six magnetic sites but for the cases reported in this paper only one site in the ethyl sulfates was observed.

## IV. EXPERIMENTAL RESULTS AND COMPARISON TO THEORY

### A. $Ce^{3+}$ in YES

We have already discussed in Sec. II the crystal field splitting of the free-ion ground state $4f^1\,{}^2F_{5/2}$ for $Ce^{3+}$ in YES, as shown in Fig. 1. We found the paramagnetic-resonance spectrum to consist of a single line, for which $g_{\parallel}=3.810\pm 0.005$, $g_{\perp}=0.20\pm 0.02$.

Relaxation measurements were made on a crystal of 2% $Ce^{3+}$ in YES, shown in Fig. 6; the data can be fitted by the expression

$$T_b^{-1}=1.0T^9+5.1\times 10^8\exp(-25/T)\ \text{sec}^{-1}, \qquad (15)$$

indicating a dominant Orbach process and a weaker and less well determined Raman process. The value of $\Delta/k$ can be determined to $\pm 1$°K by our measurements. Spin-lattice relaxation measurements have previously been reported for both $Ce^{3+}$ in LaES[2] and the concentrated CeES salt.[5]

The $g$-factors are given by $g_{\parallel}=2\Lambda|\langle i|J_z|i\rangle|$ and $g_{\perp}=2\Lambda|\langle i|J_x|j\rangle|$, where $|i\rangle$ and $|j\rangle$ are a Kramers doublet, and $\Lambda=6/7$ is the Landé $g$ factor. In first order, neglecting admixtures from the ${}^2F_{7/2}$ multiplet, the axial field of $C_{3h}$ symmetry cannot admix the $|J_z\rangle$ states in this lowest $J=\frac{5}{2}$ multiplet. The Kramers

[26] E. H. Erath, J. Chem. Phys. 34, 1985 (1961).
[27] A. Zalkin, J. D. Forrester, and D. H. Templeton, J. Chem. Phys. 39, 2881 (1963).
[28] J. A. A. Ketelaar, Physica 4, 619 (1937); D. R. Fitzwater and R. E. Rundle, Z. Krist. 112, 362 (1959).

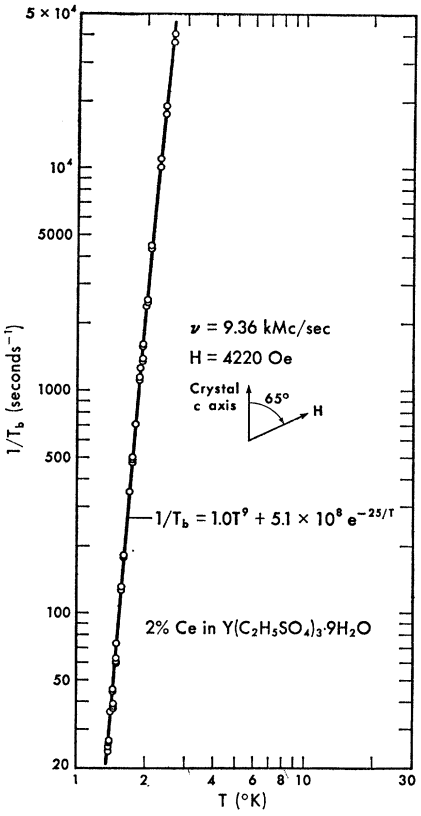


FIG. 6. Observed relaxation rate $T_1^{-1}$ versus $T$ for 2% $Ce^{3+}$ in YES, showing a Raman and an Orbach process.

doublets are thus

$$|a\rangle=|-\tfrac{5}{2}\rangle, \quad (16a)$$

$$|b\rangle=|\tfrac{5}{2}\rangle, \quad (16b)$$

yielding $g_{\parallel}=4.29$, $g_{\perp}=0$;

$$|c\rangle=|-\tfrac{1}{2}\rangle, \quad (16c)$$

$$|d\rangle=|\tfrac{1}{2}\rangle, \quad (16d)$$

yielding $g_{\parallel}=0.857$, $g_{\perp}=2.57$; and

$$|e\rangle=|-\tfrac{3}{2}\rangle, \quad (16e)$$

$$|f\rangle=|\tfrac{3}{2}\rangle, \quad (16f)$$

yielding $g_{\parallel}=2.57$, $g_{\perp}=0$. We thus tentatively identify Eqs. (16a), (16b) as the ground state and explain below the observed $g$ factors. We note that for $Ce^{3+}$ diluted in LaES[29] there is an excited doublet at $\Delta/hc=3.94$ $cm^{-1}$ described by Eqs. (16a), (16b), and a ground state described by Eqs. (16c), (16d). Thus there is the rather unusual result that the two lowest doublets are inverted and also $\Delta$ is much changed between YES and LaES. However, in concentrated CeES[30] the lowest doublet is described by $J_z=\pm\frac{5}{2}$.

[29] D. P. Devor and R. H. Haskins, Bull. Am. Phys. Soc. 6, 364 (1961).

[30] G. S. Bogle, A. H. Cooke, and S. Whitley, Proc. Phys. Soc. (London) A64, 931 (1951).

Since the static crystal field parameters have not been determined experimentally for Ce in YES, LaES, or even for concentrated CeES we first proceed by extrapolating the parameters given in Fig. 2, finding

$$A_2^0\langle r^2\rangle\approx 32 \text{ cm}^{-1},$$
$$A_4^0\langle r^4\rangle\approx -95 \text{ cm}^{-1},$$
$$A_6^0\langle r^6\rangle\approx -55 \text{ cm}^{-1},$$
$$A_6^6\langle r^6\rangle\approx 800 \text{ cm}^{-1}. \quad (17a)$$

One should not expect these values to be quite correct for $Ce^{3+}$ in YES, for several reasons: First, the molecular volumes of LaES and CeES are more than 3% larger than that for YES,[28] while the three water molecules nearest the rare-earth ion are about 4% farther away in CeES than in YES. Thus, the $Ce^{3+}$ ion should see a stronger field in YES than in LaES or CeES, since elementary calculations show $A_n^0\propto 1/a^{n+1}$, where $a$ is the interatomic distance to the ligands. Still confining our attention to the lowest multiplet $J=\frac{5}{2}$, we note further than the splitting between the lowest doublets is given by

$$E_{\pm 1/2}-E_{\pm 5/2}=1.03A_2^0\langle r^2\rangle+0.381A_4^0\langle r^4\rangle. \quad (17b)$$

Using the extrapolated values Eq. (17a) in Eq. (17b) yields $E_{\pm 1/2}-E_{\pm 5/2}=-3.24$ $cm^{-1}$, indicating that the $J_z=\pm\frac{1}{2}$ doublet is lowest; this actually agrees quite well with the measured splitting of 3.94 $cm^{-1}$ for $Ce^{3+}$ in LaES.

It is possible to explain both the value of $\Delta$ and the $g$ factors observed for $Ce^{3+}$ in YES by assuming that in addition to crystal field terms of Eq. (17a), corresponding to $C_{3h}$ symmetry, we have a term $A_4^3\langle r^4\rangle=+84.1$ $cm^{-1}$ corresponding to a small $C_{3v}$ distortion.[17] This particular value yields the new ground states

$$|a\rangle=0.952|-\tfrac{5}{2}\rangle+0.306|\tfrac{1}{2}\rangle, \quad (18a)$$

$$|b\rangle=0.952|\tfrac{5}{2}\rangle-0.306|-\tfrac{1}{2}\rangle, \quad (18b)$$

for which $g_{\parallel}=3.80$, $g_{\perp}=0.20$, which are quite close to the observed values; inclusion of this $A_4^3$ term also puts the first excited state at $\Delta/hc=17.4$ $cm^{-1}$, corresponding to $\Delta/k=25°K$, with wave functions given by

$$|c\rangle=0.306|-\tfrac{5}{2}\rangle-0.952|\tfrac{1}{2}\rangle, \quad (19a)$$

$$|d\rangle=0.306|\tfrac{5}{2}\rangle+0.952|-\tfrac{1}{2}\rangle, \quad (19b)$$

yielding $g_{\parallel}=0.38$ and $g_{\perp}=2.36$. Attempts to observe directly the paramagnetic resonance of the excited state were unsuccessful. An alternative explanation of the observed $\Delta$ and the $g$ factors for $Ce^{3+}$ in YES could no doubt be derived assuming admixtures from the upper $^2F_{7/2}$ multiplet.

Using Eq. (17a), with the wave functions Eqs. (18a), (18b), Eqs. (19a), (19b), and Eqs. (16e), (16f), the crystal density $\rho=1.8$ g $cm^{-3}$ and $v=2.0\times 10^5$ cm/sec, and scheme Eq. (8) we thus calculate from

Eqs. (11), (12), and (14) the relaxation rate of $Ce^{3+}$ in YES,

$$T_1^{-1}=0.56T+0.57\times10^{-3}T^9+7.54\times10^8 \times\exp(-25/T)\ \text{sec}^{-1}, \quad (20)$$

for the explicit case of Fig. 6. The alternative scheme Eq. (7) yields

$$T_1^{-1}=19.6T+0.83T^9+2.87\times10^{10} \times\exp(-25/T)\ \text{sec}^{-1}. \quad (21)$$

If, instead, we use the wave functions Eq. (16) we find for scheme Eq. (8)

$$T_1^{-1}=0.048T+1.8\times10^{-4}T^9+4.1\times10^8 \times\exp(-25/T)\ \text{sec}^{-1}, \quad (22a)$$

and for scheme Eq. (7)

$$T_1^{-1}=3.39T+1.0T^9+3.2\times10^{10} \times\exp(-25/T)\ \text{sec}^{-1}. \quad (22b)$$

Either Eqs. (20) or (22a) give a good explanation of the observed Orbach relaxation data; the Raman rate is in better agreement with Eqs. (21) or (22b). The direct process is too weak to be observed.

We note that Eqs. (18) and (19) are the eigenfunctions of the spin-orbit and crystal-field interactions; as such they are sufficient for evaluating Eqs. (10b), (12a), (13), and (14). However, in evaluating Eq. (11) for the direct process in a Kramers doublet we require nondegenerate basic functions, and so we have always used combinations of $|a\rangle$ and $|b\rangle$, etc., for the other doublets, which are eigenfunctions of the Zeeman perturbation $\Lambda\beta\mathbf{H}\cdot\mathbf{J}$ at the particular angle of interest. To be specific we replace $|a\rangle$ and $|b\rangle$ in Eq. (11) by

$$|A\rangle=\left(\frac{1}{\sqrt{2}}\right)\left[\left(1+\frac{g_{\parallel}}{g}\cos\theta\right)^{1/2}|a\rangle +\left(1-\frac{g_{\parallel}}{g}\cos\theta\right)^{1/2}|b\rangle\right]$$

$$|B\rangle=\left(\frac{1}{\sqrt{2}}\right)\left[-\left(1-\frac{g_{\parallel}}{g}\cos\theta\right)^{1/2}|a\rangle +\left(1+\frac{g_{\parallel}}{g}\cos\theta\right)^{1/2}|b\rangle\right], \quad (23)$$

where $\theta=\angle z$, $H$ and $g^2=g_{\parallel}^2\cos^2\theta+g_{\perp}^2\sin^2\theta$.

### B. $Pr^{3+}$ in YES and LaES

The paramagnetic resonance spectrum of $Pr^{3+}$ ($4f^2$, $^3H_4$) in LaES[31] and in YES[32] is essentially the same, consisting of 6 broad hyperfine (hfs) lines due to the 100% abundant isotope $Pr^{141}$ ($I=\frac{5}{2}$). Our relaxation

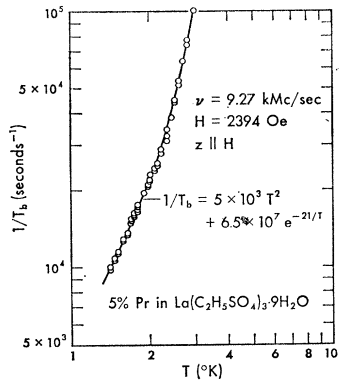


FIG. 7. Relaxation rate versus $T$ for $Pr^{3+}$ in LaES, showing a bottlenecked direct process $\propto T^2$ and an Orbach process.

time measurements made at any point within the linewidth (500 Oe) on a given hfs line yielded the same time constant. The data for the $m_I=\frac{3}{2}$ line for a single crystal (average thickness$\approx$2 mm) of 5% $Pr^{3+}$ in LaES are given in Fig. 7, to which has been fitted the expression

$$T_b^{-1}=5\times10^3T^2+6.5\times10^7\exp(-21/T)\ \text{sec}^{-1}, \quad (24)$$

where the exponent is determined to an accuracy of $\Delta/k=21\pm4$°K. Thus, instead of a direct process linearly dependent on $T$, we find a phonon bottleneck proportional to $T^2$ as in Eq. (10a). The Orbach term is not very accurately determined, the pertinent data being over only a narrow temperature range.

Data taken on a crystal of 5% $Pr^{3+}$ in YES, where $m_I=-\frac{5}{2}$, $\nu=9.40$ Gc/sec, $H=7010$ Oe, and $z\|H$ could be reasonably fit to the expression

$$T_b^{-1}=4.1\times10^3T^2+3.8\times10^7\exp(-19/T)\ \text{sec}^{-1}, \quad (25)$$

where the exponent is experimentally determined to the accuracy $\Delta/k=19\pm5$°K. The second term in Eq. (25) can be replaced by a Raman term 30 $T^7$, with an equally good fit, however. Likewise for the data of Fig. 7; thus although the data are accurate to within 5%, this is not quite good enough to determine whether the rapid process is Orbach or Raman. The data for Pr: LaES can also be fitted to the expression $T_1^{-1}=4.9$

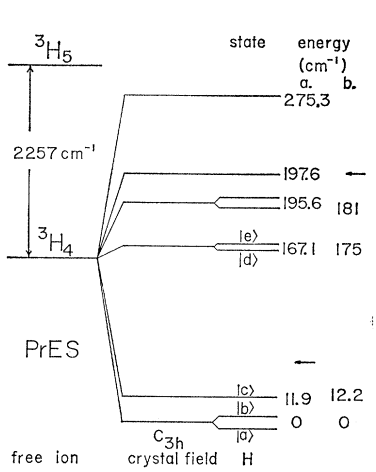


FIG. 8. Energy levels of concentrated PrES showing the crystal-field splitting of the $^3H_4$ ground state, as given by (a) Hüfner (Ref. 23) and (b) Gruber (Ref. 33).

[31] B. Bleaney and H. E. D. Scovil, Phil. Mag. **43**, 999 (1952).
[32] J. M. Baker and B. Bleaney, Proc. Roy. Soc. (London) **A245**, 156 (1958).

$\times 10^3 T^2 + 16T^7 + 1.2\times 10^9 \exp(-32/T)$ sec$^{-1}$ but this value of $\Delta$ is considerably larger than the value $\Delta/k \approx 17$°K in PrES. This is shown in the energy level diagram for concentrated PrES in Fig. 8, showing the optically measured splittings[23,33] which indicate a singlet $|c\rangle$ as the first excited state at $\Delta_1/hc \cong 12$ cm$^{-1}$. we take as wave functions[32]

$$|a\rangle = 0.914|2\rangle - 0.407|-4\rangle, \quad (26a)$$

$$|b\rangle = 0.914|-2\rangle - 0.407|4\rangle, \quad (26b)$$

$$|c\rangle = 0.707(|3\rangle - |-3\rangle), \quad (26c)$$

$$|d\rangle = 0.407|-2\rangle + 0.914|4\rangle, \quad (26d)$$

$$|e\rangle = 0.407|2\rangle + 0.914|-4\rangle, \quad (26e)$$

where Eqs. (26a), (26b) give $g_{\parallel} = 1.62$, $g_{\perp} = 0$, compared to the measured values[32] of $g_{\parallel} = 1.525 \pm 0.02$, $g_{\perp} = 0$, for YES,[32] and $g_{\parallel} = 1.69 \pm 0.01$, $g_{\perp} = 0$ for LaES.[31] The crystal-field parameters found by Gruber[33] for PrES are $A_2^0\langle r^2\rangle = 15.3$ cm$^{-1}$, $A_4^0\langle r^4\rangle = -88.3$ cm$^{-1}$, $A_6^0\langle r^6\rangle = -48.76$ cm$^{-1}$, and $A_6^6\langle r^6\rangle = 548.48$ cm$^{-1}$ as shown in Fig. 2. Calculation of the various processes, with $z \| H$, and using scheme Eq. (7), gives

$$T_1^{-1} = 5\times 10^5 T + 1.7T^7 + 4.2\times 10^9 \times \exp(-20/T) \text{ sec}^{-1}, \quad (27)$$

while using scheme Eq. (8) gives

$$T_1^{-1} = 3.6\times 10^4 T + 6.2\times 10^{-3} T^7 + 5.9\times 10^7 \times \exp(-20/T) \text{ sec}^{-1}, \quad (28)$$

where in both calculations we have used the splitting $\Delta/k = 20$°K. In either case the direct process is strong enough to be consistent with the observed bottleneck, since $AT \gg DT^2$. If the relaxation is really by the Orbach process then scheme Eq. (8) agrees best with the data, Eq. (25).

No comparison can be made between theory and experiment for the direct process since it is bottle-necked, but we can use the data to estimate the phonon lifetime $T_{\rm ph}$. Equation (10a) can be rewritten as [cf. S&J Eq. (38a)]

$$\frac{1}{T_b} = \frac{1}{T_{\rm ph}} \frac{6k^2\beta g(\Delta H)}{\pi^2\hbar^3 c v^3} T^2 \equiv DT^2 \text{ sec}^{-1}, \quad (29)$$

where $\Delta H$ is the EPR linewidth, and $g$ is the "effective" $g$ factor of the line. We evaluate Eq. (29) for our case using $v = 2.0\times 10^5$ cm/sec for the ethyl sulfates, $g = 2.76$, $c = 1.82\times 10^{19}$ cm$^{-3}$ (we have divided the $Pr^{3+}$ concentration by six since we consider only one of the six hfs lines), $\Delta H = 500$ Oe, to find

$$\frac{1}{T_b} = \frac{8.68\times 10^{-4}}{T_{\rm ph}} T^2 \text{ sec}^{-1}. \quad (30)$$

If we define a mean free phonon path $\bar{l} = T_{\rm ph} v$, this together with the measured value $D = 5\times 10^3$ sec$^{-1}$ (°K)$^{-2}$ yields $\bar{l} = 0.35$ mm. This is an order of magnitude smaller than our average crystal thickness of $\approx 2$ mm. Our result roughly indicates that the hot phonons are not getting to the surface or else that the effective spin-phonon linewidth $\Delta H$ is much greater than the EPR linewidth.

Another feature worth discussing is the heating effects we observed at temperatures just above the $He^4$ $\lambda$ point (2.17°K). During some of the initial measurements on a LaES crystal containing 5% $Pr^{3+}$ we found a discontinuity in the measured relaxation time as we passed through the $\lambda$ point as illustrated in Fig. 9. In taking the data no changes were made in the apparatus except the temperature. Just below the $\lambda$ point the observed relaxation time was $\sim 35$ $\mu$sec, as seen from Fig. 9; but as the He warmed up through $T = 2.17$°K, the decay abruptly lengthened, giving a time constant of $\sim 37$ msec. This discontinuity was independent of pulse repetition rate, but quite dependent on pulse power $\times$ pulse width, i.e., on the energy pumped into the spin system during the pulse. We attribute this spurious effect to crystal heating due to the sudden change, by a factor of $\sim 10^6$, in thermal conductivity of the He bath at the $\lambda$ point. It apparently is related to other similar effects.[34] Later measurements were always made with sufficiently low power and short pulse length so as to hold the crystal at the helium-bath temperature.

### C. $Nd^{3+}$ in YES

We found the paramagnetic resonance spectrum of $Nd^{3+}$ ($4f^3$, $^4I_{9/2}$) in YES to be nearly identical to that of $Nd^{3+}$ in LaES,[35] consisting of a strong central line

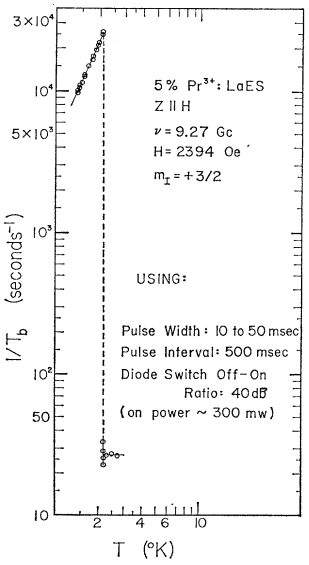


FIG. 9. Diagram showing the large discontinuity in the relaxation rate observed at the $\lambda$ point of liquid helium when large saturating microwave power is used.

[33] J. B. Gruber, J. Chem. Phys. 38, 946 (1963).

[34] D. J. Griffiths, Thesis, University of British Columbia, 1965 (unpublished); R. J. R. Hayward and D. E. Dugdale, Phys. Letters 12, 88 (1964).

[35] B. Bleaney, H. E. D. Scovil, and R. S. Trenam, Proc. Roy. Soc. (London) A223, 15 (1954).

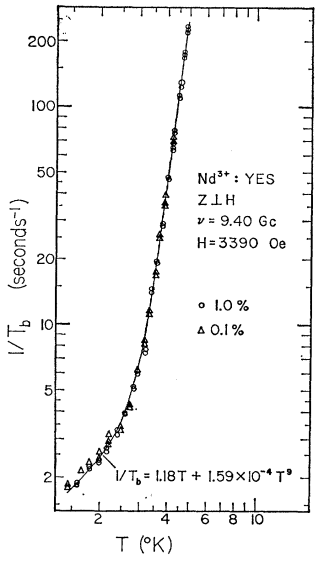


FIG. 10. Relaxation rate versus $T$ for $Nd^{3+}$ in YES, showing a direct and a Raman process.

due to even isotopes, flanked by two sets of eight hfs of $Nd^{143}$ and $Nd^{145}$. Relaxation measurements were always made on the central line for which we found $g_{\parallel}=3.665\pm0.005$, $g_{\perp}=1.980\pm0.005$; these are close to the values for $Nd^{3+}$ in LaES (Ref. 35): $g_{\parallel}=3.535$, $g_{\perp}=2.073$.

Relaxation-time data taken for a crystal of 1% $Nd^{3+}$ in YES, oriented with $z\perp\mathbf{H}$, are shown in Fig. 10 and are fitted by the expression

$$T_b^{-1}=1.2T+1.64\times10^{-4}T^9\ \text{sec}^{-1}, \tag{31}$$

clearly showing a direct and a Raman process. Data for a crystal of 0.1% $Nd^{3+}$ in YES are also shown in Fig. 10. There is no observable dependence on concentration as expected for the true direct and Raman processes. Spin-lattice relaxation measurements have previously been reported for both $Nd^{3+}$ in LaES[2] and the concentrated NdES salt.[5]

The energy-level diagram shown in Fig. 11 for NdES[36] indicates a first excited doublet $\Delta/hc=149\ \text{cm}^{-1}$, much too high to lead to an Orbach process. The wave functions calculated from the measured crystal field parameters[36] are given by

$$|a\rangle=0.919|-\tfrac{7}{2}\rangle+0.382|\tfrac{5}{2}\rangle, \tag{32a}$$

$$|b\rangle=0.919|\tfrac{7}{2}\rangle+0.382|-\tfrac{5}{2}\rangle, \tag{32b}$$

$$|c\rangle=|-\tfrac{1}{2}\rangle, \tag{32c}$$

$$|d\rangle=|\tfrac{1}{2}\rangle, \tag{32d}$$

$$|e\rangle=0.749|-\tfrac{9}{2}\rangle+0.665|\tfrac{3}{2}\rangle, \tag{32e}$$

$$|f\rangle=0.749|\tfrac{9}{2}\rangle+0.665|-\tfrac{3}{2}\rangle. \tag{32f}$$

Equations (32a) and (32b) yield $g_{\parallel}=3.7$, $g_{\perp}=2.0$, in good agreement with the measured values. If we use the parameters[36] $A_2^0\langle r^2\rangle=58.4\ \text{cm}^{-1}$, $A_4^0\langle r^4\rangle=-68.2\ \text{cm}^{-1}$, $A_6^0\langle r^6\rangle=-42.7\ \text{cm}^{-1}$, and $A_6^6\langle r^6\rangle=595\ \text{cm}^{-1}$, as shown in Fig. 2, we find, with $z\perp H$, using scheme Eq. (7)

$$T_1^{-1}=0.74T+3.4\times10^{-5}T^9\ \text{sec}^{-1}. \tag{33}$$

This is felt to be in satisfactory agreement with Eq. (31), considering the many approximations in the theory. If on the other hand we use scheme Eq. (8) to perform the calculation we find

$$T_1^{-1}=0.24T+3.3\times10^{-6}T^9\ \text{sec}^{-1}. \tag{34}$$

### D. $Sm^{3+}$ in LaMN

The paramagnetic resonance spectrum of $Sm^{3+}$ ($4f^5$, $^6H_{5/2}$) in LaMN is the same as that for concentrated SmMN reported by Cooke and Duffus.[37] In the dilute salt S&J find $g_{\parallel}=0.736\pm0.005$, $g_{\perp}=0.363\pm0.10$.

Relaxation time measurements made on a concentrated crystal of SmMN by S&J indicated a bottlenecked direct process and a Raman process:

$$T_b^{-1}=1.32T^2+5\times10^{-2}T^9\ \text{sec}^{-1}. \tag{35}$$

They also took data for 0.05% $Sm^{3+}$ in LaMN but only over a limited temperature range, finding

$$T_b^{-1}=8T+4\times10^{-3}T^9\ \text{sec}^{-1}. \tag{36}$$

We have made supplementary measurements on $Sm^{3+}$ in a LaMN crystal grown from a 10% solution of Sm in LaMN, for which line intensity measurements indicate an actual $Sm^{3+}$ concentration of $\sim1\%$. The data from these measurements, with $z\|\mathbf{H}$, is plotted in Fig. 12 and is fitted by the expression

$$T_b^{-1}=3.4T+1.3\times10^{-2}T^9+1.6\times10^{10}\times\exp(-55/T)\ \text{sec}^{-1}, \tag{37}$$

where the value $\Delta/k$ is determined to $\pm3$°K. The high-temperature data clearly indicate a Raman term plus an Orbach term corresponding to a level at

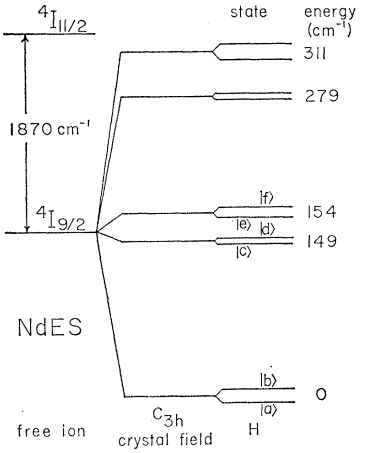


FIG. 11. Energy levels of concentrated NdES showing the crystal-field splitting of the $^4I_{9/2}$ ground state, as measured by Gruber and Satten (Ref. 36).

[36] J. B. Gruber and R. A. Satten, J. Chem. Phys. 39, 1455 (1963).

[37] A. H. Cooke and H. J. Duffus, Proc. Roy. Soc. (London) A229, 407 (1955).

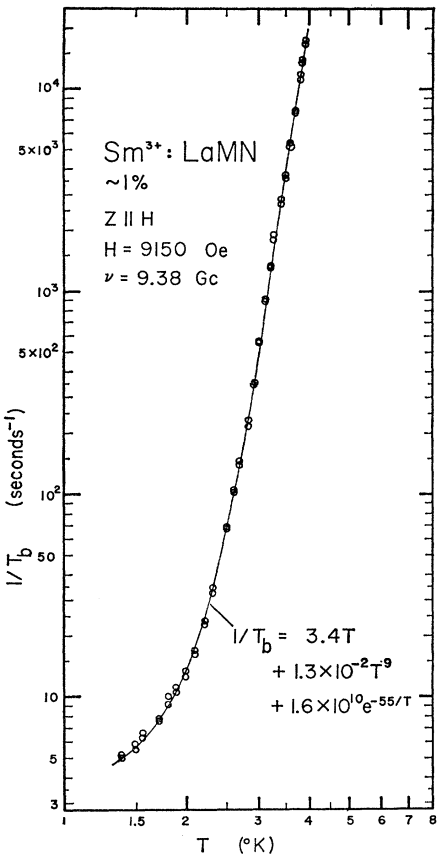


FIG. 12. Relaxation rate versus $T$ for $Sm^{3+}$ in LaMN for a crystal grown from a solution 10% by volume of SmMN in LaMN, showing direct, Raman, and Orbach terms.

$\Delta_1/hc=38$ cm$^{-1}$, which probably corresponds to the level at 46.5 cm$^{-1}$ observed for concentrated SmMN.[38]

We take as wave functions those from S&J,

$$|a\rangle=0.749|-\tfrac{5}{2}\rangle+0.665|\tfrac{1}{2}\rangle, \quad (38a)$$

$$|b\rangle=0.749|\tfrac{5}{2}\rangle-0.665|-\tfrac{1}{2}\rangle, \quad (38b)$$

$$|c\rangle=|-\tfrac{3}{2}\rangle, \quad (38c)$$

$$|d\rangle=|\tfrac{3}{2}\rangle, \quad (38d)$$

$$|e\rangle=0.665|-\tfrac{5}{2}\rangle-0.749|\tfrac{1}{2}\rangle, \quad (38e)$$

$$|f\rangle=0.665|\tfrac{5}{2}\rangle+0.749|-\tfrac{1}{2}\rangle, \quad (38f)$$

where $|a\rangle$ and $|b\rangle$ give $g_{\parallel}=0.67$, $g_{\perp}=0.382$ for the ground doublet. The crystal-field parameters deduced from the optical data[38] are $A_2{}^0\langle r^2\rangle\approx-14$ cm$^{-1}$, $A_4{}^0\langle r^4\rangle\approx-15$ cm$^{-1}$, and $A_4{}^3\langle r^4\rangle\approx\pm1440$ cm$^{-1}$. If we take the crystal density $\rho=2.0$ g cm$^{-3}$, $v=2.5\times10^5$ cm sec$^{-1}$, and use our experimental value $\Delta_1/k=55$°K, we calculate, with $z\|\mathbf{H}$, and scheme Eq. (7)

$$T_1{}^{-1}=0.34\times10^{-1}T+1.5\times10^{-7}T^9+4.4\times10^8\times\exp(-55/T)\ \text{sec}^{-1}. \quad (39)$$

This is in very poor agreement with the data of Eq. (37). However, S&J show that admixtures from the $^6H_{7/2}$ multiplet using a parameter such as $A_6{}^6\langle r^6\rangle\approx2000$ cm$^{-1}$ can produce matrix elements 10 times larger than those found in first order using only the $^6H_{5/2}$ level. We thus feel justified in multiplying our previous values of $\sum_{nm}|\langle a|v_n{}^m|c\rangle|^2$, by roughly a factor $10^2$, which will then give the order of magnitude estimate:

$$T_1{}^{-1}\sim3.4T+1.5\times10^{-3}T^9+4.4\times10^{10}\times\exp(-55/T)\ \text{sec}^{-1}, \quad (40)$$

which agrees substantially better term by term with the data than Eq. (39).

### E. $Sm^{3+}$ in LaES

We have made relaxation-time measurements on the strong central line of the paramagnetic resonance

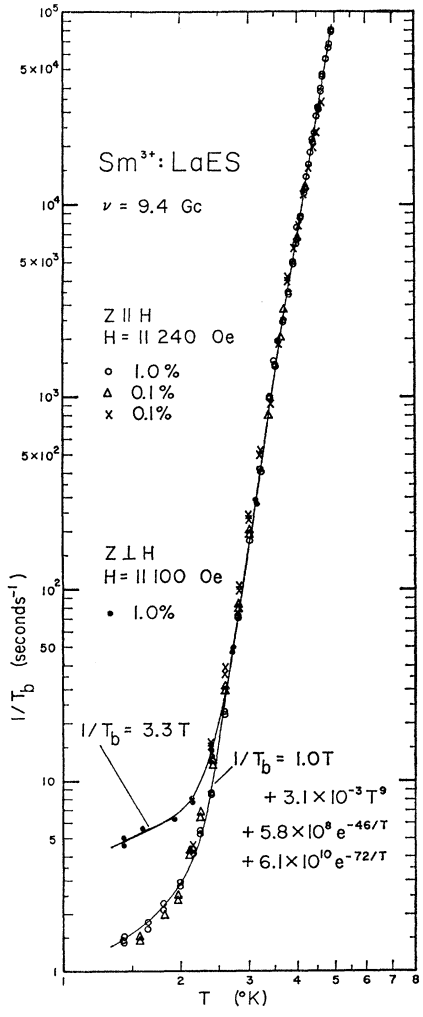


FIG. 13. Relaxation rate versus $T$ for $Sm^{3+}$ in LaES, showing direct, Raman, and Orbach processes. The second Orbach term becomes dominant only at the highest temperatures.

[38] A. Friederich, K. H. Hellwege, and H. Lämmermann, Z. Physik **159**, 524 (1960).

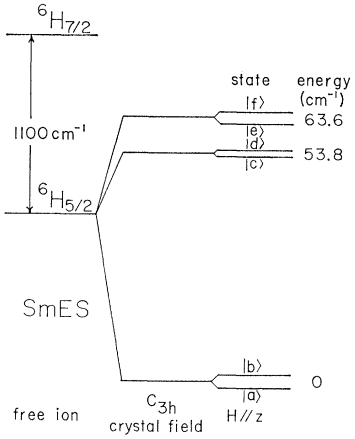


FIG. 14. Energy levels of concentrated SmES showing the crystal-field splitting of the $^6H_{5/2}$ ground state, as taken from Hüfner (Ref. 23).

spectrum[39] due to the even isotopes of $Sm^{3+}$ in LaES for crystals containing 1% and 0.1% of the magnetic ion. The data with $z\|H$ are given in Fig. 13, and are found to fit the expression

$$T_b^{-1}=1.0T+3.1\times10^{-3}T^9+5.8\times10^8\exp(-46/T)+6.1\times10^{10}\exp(-72/T)\ \text{sec}^{-1}, \quad (41)$$

where the estimated errors in the exponentials are $\Delta_1/k=46\pm2$°K and $\Delta_2/k=72\pm10$°K. For $z\perp H$, we find the direct process to be $T_{1d}^{-1}=3.3T$ sec$^{-1}$ but the Raman and Orbach terms are unchanged as expected. The large error in $\Delta_2$, due to the small temperature range over which it can be measured, results roughly in an order of magnitude uncertainty in the coefficient $B$. The energy levels of concentrated SmES,[23] Fig. 14, indicate a Kramers doublet at $\Delta_1/hc=53.8$ cm$^{-1}$ and at $\Delta_2/hc=63.6$ cm$^{-1}$, so high that an Orbach process would not be normally expected. However, the data of Fig. 13 definitely require, in addition to the Raman and first Orbach term which provide a good fit to the data below ~3.8°K, some additional term above ~3.8°K. There seems to be a definite break in the data around 3.8°K, as shown by the semilog plot of Fig. 15, which shows two straight lines with two different slopes. We have interpreted this result as two Orbach terms; the second term becomes dominant only at the higher temperatures. Both 1 and 0.1% crystals showed this same behavior. This result suggests that the levels $\Delta_1/hc=53.8$ cm$^{-1}$ and $\Delta_2/hc=63.6$ cm$^{-1}$ in SmES are shifted to the values $32\pm2$ cm$^{-1}$ and $50\pm7$ cm$^{-1}$ in the dilute salt.

Some spurious effects in the relaxation measurements made on this salt are of interest. With short saturating pulses (~10 μsec) the signal recovery seemed to be nearly exponential, but the dominant time constant was found to be quite dependent on pulse width and pulse power for all temperatures. Unless pulse widths of at least 1 msec in length and pulse power of about 15 mW were used, the major recovery occurred in a short variable spectral diffusion[40] time rather than in the longer spin-lattice time. Actually this is a general feature of pulse-recovery measurements on all salts, but was particularly noticeable for $Sm^{3+}$ in LaES. Thus, a short or weak saturating pulse will result in some degree of saturation in only part of the inhomogeneous line, after which the process of spectral diffusion quickly brings the entire line to a common temperature; then spin-lattice relaxation brings the entire line to the bath temperature. One thus sees some of the signal recover quickly, followed by a final slower recovery. If the pulse width or power is increased the spectral diffusion (i.e., cross relaxation) can take place during the pulse, the entire line can thus be saturated, and the major recovery observed is due solely to spin-lattice relaxation. It is always necessary to show experimentally that the recorded relaxation rate is independent of pulse power and width.

If we neglect admixtures from the $^6H_{7/2}$ multiplet level we have for the ground-state multiplet $^6H_{5/2}$ three Kramers doublets:

$$|a\rangle=|-\tfrac{1}{2}\rangle, \quad (42a)$$
$$|b\rangle=|\tfrac{1}{2}\rangle, \quad (42b)$$
$$|c\rangle=|-\tfrac{3}{2}\rangle, \quad (42c)$$
$$|d\rangle=|\tfrac{3}{2}\rangle, \quad (42d)$$
$$|e\rangle=|-\tfrac{5}{2}\rangle, \quad (42e)$$
$$|f\rangle=|\tfrac{5}{2}\rangle, \quad (42f)$$

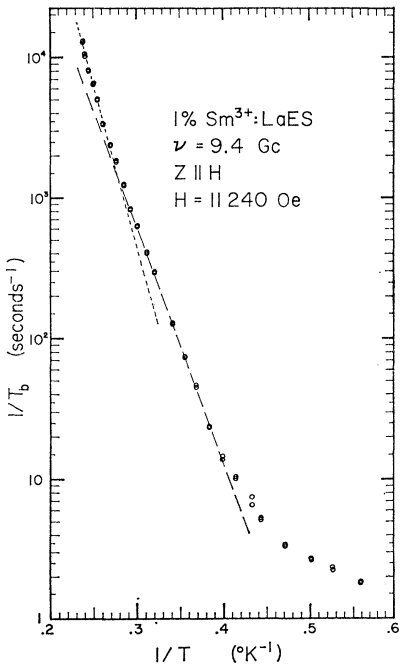


FIG. 15. Relaxation rate versus $1/T$ for $Sm^{3+}$ in LaES, plotted on semilog paper, showing the evidence for two Orbach processes via two different excited states.

[39] G. S. Bogle and H. E. D. Scovil, Proc. Phys. Soc. (London) **A65**, 368 (1952).

[40] K. D. Bowers and W. B. Mims, Phys. Rev. **115**, 285 (1959); W. B. Mims, K. Nassau, and J. D. McGee, *ibid.* **123**, 2059 (1961).

where $|a\rangle$ and $|b\rangle$ give $g_{\parallel}=0.286$, $g_{\perp}=0.857$ compared to the measured values,[39] $g_{\parallel}=0.596$, $g_{\perp}=0.604$. Elliott and Stevens[19] show that small admixtures from the $^6H_{7/2}$ level into Eqs. (42a), (42b) produce a large change in the $g$ factors, and we will consider this effect later. If we take the values[23] $A_2{}^0\langle r^2\rangle=78$ cm$^{-1}$ and $A_4{}^0\langle r^4\rangle=-53$ cm$^{-1}$, which are given in Fig. 2, and use Eq. (8a) with $z\|\mathbf{H}$ we calculate from Eqs. (12a) and (14) the values

$$T_1^{-1}=0.89\times10^{-5}T^9+1.51\times10^9\exp(-46/T)+3.10\times10^9\exp(-72/T)\ \text{sec}^{-1}. \quad (43)$$

The direct process vanishes because $J_z$ does not connect the ground doublet with the two higher doublets [cf. Eq. (11)]. However, for $z\perp H$, it does, and Eq. (11) yields $T_{1d}^{-1}=0.69T$ sec$^{-1}$. Doing the same calculation with scheme Eq. (7) gives, for $z\|H$,

$$T_1^{-1}=3.68\times10^{-4}T^9+1.75\times10^{10}\exp(-46/T)+5.4\times10^{10}\exp(-72/T)\ \text{sec}^{-1}. \quad (44)$$

For $z\perp H$, Eq. (7) yields for the direct processes $T_{1d}^{-1}=6.1T$ sec$^{-1}$. The first Orbach process in Eq. (43) agrees within a factor of 3 with experiment, but the other processes are quite far off. Except for the first Orbach term, Eq. (44) fits the data better.

Huang[10] has also reported relaxation rate measurements for $Sm^{3+}$ in LaES; he finds no Orbach terms, but direct and Raman terms an order of magnitude larger than our data, Fig. 13. We have no explanation of this discrepancy other than the following: by using short, weak pulses, as noted above, we were able to observe shorter relaxation times, but believe that they represent spectral diffusion rather than the true spin lattice relaxation time.

Elliott and Stevens[19] have pointed out that it is possible to explain the observed $g$ factors by inclusion of admixtures from the $^6H_{7/2}$ multiplet level. Thus the doublet $|a\rangle$, $|b\rangle$ of Eqs. (42a), (42b) becomes

$$|a\rangle'=0.997|\tfrac{5}{2},\tfrac{1}{2}\rangle+0.0715|\tfrac{7}{2},\tfrac{1}{2}\rangle, \quad (45a)$$

$$|b\rangle'=0.997|\tfrac{5}{2},-\tfrac{1}{2}\rangle-0.0715|\tfrac{7}{2},-\tfrac{1}{2}\rangle, \quad (45b)$$

which yields $g_{\parallel}=0.675$, $g_{\perp}=0.643$, which are in fair agreement with the observed values $g_{\parallel}=0.596$, $g_{\perp}=0.604$. We wish to point out that by further assuming a term $A_4{}^3\langle r^4\rangle$, as was done in Sec. IV, $A$ for $Ce^{3+}$ in YES, it is possible to explain exactly the observed $g$ factors. We find that the following representative values, $A_2{}^0\langle r^2\rangle\sim45$ cm$^{-1}$, $A_4{}^0\langle r^4\rangle\sim-25$ cm$^{-1}$, $A_6{}^0\langle r^6\rangle\sim-30$ cm$^{-1}$, $A_6{}^6\langle r^6\rangle\sim450$ cm$^{-1}$, and $A_4{}^3\langle r^4\rangle\sim360$ cm$^{-1}$ will give a ground doublet that explains exactly the observed $g$ values and will also explain the crystal field splittings $\Delta_1=46$ cm$^{-1}$ and $\Delta_2=72\pm10$ cm$^{-1}$ given in Eq. (41). These parameters are all smaller than any corresponding values extrapolated in Fig. 2 for $Sm^{3+}$ and thus are consistent with the weaker crystal field the $Sm^{3+}$ ion should see in a LaES lattice as opposed to a smaller ($\sim3\%$) SmES lattice.

Although the inclusion of admixtures from the $^6H_{7/2}$ multiplet is essential to an understanding of the relaxation of $Sm^{3+}$ in LaMN as we have noted in Sec. IV D, it is probably not essential for $Sm^{3+}$ in LaES except for the direct process with $z\|H$, as Orbach has pointed out.[41] He calculates $T_{1d}^{-1}=0.029T$ sec$^{-1}$ for $z\|H$ at the field $H=11.2$ kOe at which our data, Fig. 13, are taken; for $z\perp H$, he calculates $T_{1d}^{-1}=0.16T$ sec$^{-1}$.

### F. $Sm^{3+}$ in YES

We observed the paramagnetic resonance spectrum of a crystal of 1% $Sm^{3+}$ in YES, finding $g_{\parallel}=0.616\pm0.002$ and $g_{\perp}=0.594\pm0.002$. Relaxation time measurements on this crystal, with $z\|H$ and $z\perp H$, are shown in Fig. 16, and can be fit to the expression

$$T_b^{-1}=1.3T+4.0\times10^{-4}T^9+8.0\times10^8\times\exp(-51/T)\ \text{sec}^{-1}, \quad (46)$$

with $\sim\perp H$. For $z\|H$, the term $1.3T$ in Eq. (46) must be replaced by 0.76. The exponent is experimentally determined to be $\Delta/k=51\pm2$°K, identifying an excited doublet at $\Delta_1/hc=35.5$ cm$^{-1}$, compared to $\Delta_1/hc=53.8$ cm$^{-1}$ as shown in Fig. 14 for SmES.

Using the wave functions Eq. (42) and the crystal-field parameters for SmES,[23] along with the experi-

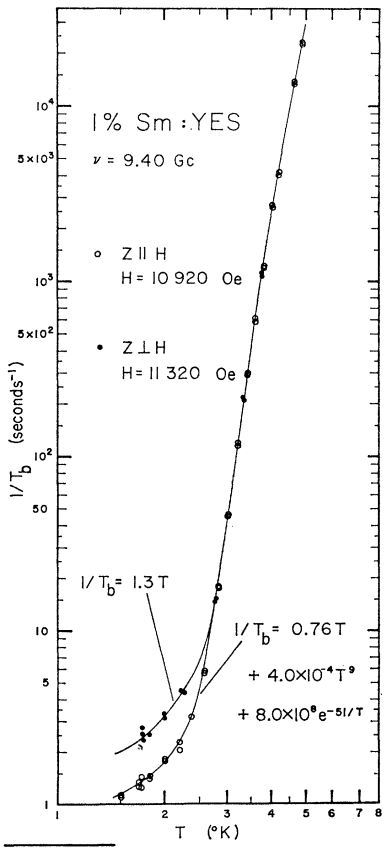


FIG. 16. Relaxation rate versus $T$ for $Sm^{3+}$ in YES, showing direct, Raman, and Orbach processes.

[41] R. Orbach, Phys. Rev. 126, 1349 (1962).

mental value $\Delta_1/hc=35.5$ cm$^{-1}$, we find for $z\perp H$, from Eqs. (12a) and (14) and scheme Eq. (8a)

$$T_1^{-1}=0.56T+1.3\times10^{-6}T^9+3.7\times10^9\times(\exp-51/T)\ \text{sec}^{-1}. \quad (47a)$$

Using scheme Eq. (7) the calculation gives

$$T_1^{-1}=5.0T+8.4\times10^{-4}T^9+2.4\times10^{10}\times\exp(-51/T)\ \text{sec}^{-1}. \quad (47b)$$

The Orbach term in Eq. (47a) is about $4\frac{1}{2}$ times larger than the experimental value given in Eq. (46), while the Raman term in Eq. (47b) provides good agreement with the corresponding term in Eq. (46).

We have made additional spin-lattice relaxation measurements on a crystal of concentrated SmES for $z\|\mathbf{H}$ at $\nu=9.4$ Gc/sec and $H=11\,015$ Oe. In this orientation the central line due to even isotopes was approximately 30 Oe wide and the remaining spectrum was clearly resolved. Our data fit quite well the expression

$$T_b^{-1}=0.25T^2+5.8\times10^{-4}T^9+9.5\times10^8\times\exp(-51/T)\ \text{sec}^{-1}, \quad (48)$$

indicating a phonon bottleneck instead of a direct process and a Raman and Orbach processes. These latter two processes in Eq. (48) are quite similar to the corresponding ones found for $Sm^{3+}$:YES given in Eq. (46), where the splitting in both cases is given by $\Delta_1/hc=35.5$ cm$^{-1}$, a value more than 30% smaller than that reported from optical measurements[23] on the concentrated SmES salt where $\Delta_1/hc=53.8$ cm$^{-1}$ as shown in Fig. 14. We have no explanation for this discrepancy.

We can estimate the size of the bottleneck coefficient $D$ from either Eq. (10a) or Eq. (29), where we take $g=0.611$, $\Delta H=30$ Oe, $v=2.0\times10^5$ cm/sec, and $c=1.3\times10^{21}$ atoms/cm$^3$ (the even isotopes which contribute to the main line are ~61% naturally abundant). Using these values and an average crystal thickness of 1 mm we estimate $D=1.57\times10^{-7}/T_{ph}=0.31$ sec$^{-1}$ (°K)$^{-2}$, since $T_{ph}=l/v=0.5\times10^{-6}$ sec. The direct process for this orientation as measured in $Sm^{3+}$:YES is $0.76T$ sec$^{-1}$ while for $Sm^{3+}$:LaES it is $1.0T$ sec$^{-1}$, so that we might expect here also a comparable rate. Thus we expect $AT>DT^2$; a bottleneck is not unexpected in concentrated SmES under these conditions.

### G. $Dy^{3+}$ in LaMN

It becomes increasingly difficult to grow the heavier rare-earth ions into the LaMN lattice. However, Park[42] was able to see a paramagnetic-resonance spectrum due to $Dy^{3+}$ in LaMN, by using crystals grown from a solution of 50% DyMN and 50% LaMN, which forces ~1% of $Dy^{3+}$ into the crystal. The EPR spectrum consists of a central line with $g_{11}=4.28\pm0.006$, $g_1=8.923\pm0.016$ due to the even isotopes, flanked by two sets of six hyperfine lines due to $Dy^{161}$ and $Dy^{163}$. We performed relaxation time measurements on a crystal grown from a 50% $Dy^{3+}$ in LaMN solution, for which line-intensity measurements indicated on actual content of ~1% $Dy^{3+}$. Measurements made on the strong central line with $z\|\mathbf{H}$ are shown in Fig. 17; the data can be fit by the single term

$$T_b^{-1}=7.0\times10^9\exp(-22.0/T)\ \text{sec}^{-1}. \quad (49)$$

This result indicates an excited state at $\Delta/hc=15.3$ cm$^{-1}$ which is responsible for an Orbach process that dominates other processes over the liquid-helium temperature range.

Judd,[24] assuming icosohedral symmetry, has given the wave functions for the ground doublet of $Dy^{3+}$ ($^4f$, $^6H_{15/2}$) in the double nitrate:

$$|a\rangle=0.274|13/2\rangle-0.706|\tfrac{7}{2}\rangle-0.436|\tfrac{1}{2}\rangle+0.476|-\tfrac{5}{2}\rangle+0.103|-11/2\rangle$$
$$|b\rangle=0.274|-13/2\rangle+0.706|-\tfrac{7}{2}\rangle-0.436|-\tfrac{1}{2}\rangle-0.476|\tfrac{5}{2}\rangle+0.103|11/2\rangle, \quad (50)$$

which yield $g_{11}=4.53$ and $g_1=9.07$; in reasonable agreement with the experimental values.

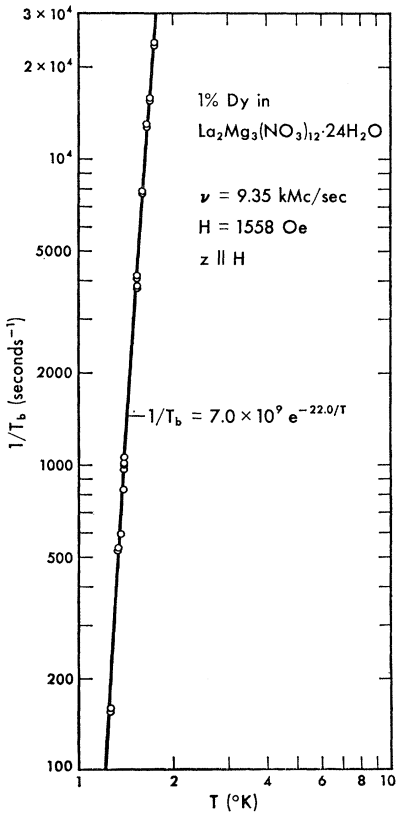


FIG. 17. Relaxation rate versus $T$ for $Dy^{3+}$ in LaMN, showing only an Orbach process. The crystal was grown from a solution of 50% DyMN and 50% LaMN, by volume.

[42] J. G. Park, Proc. Roy. Soc. (London) **A245**, 118 (1958).

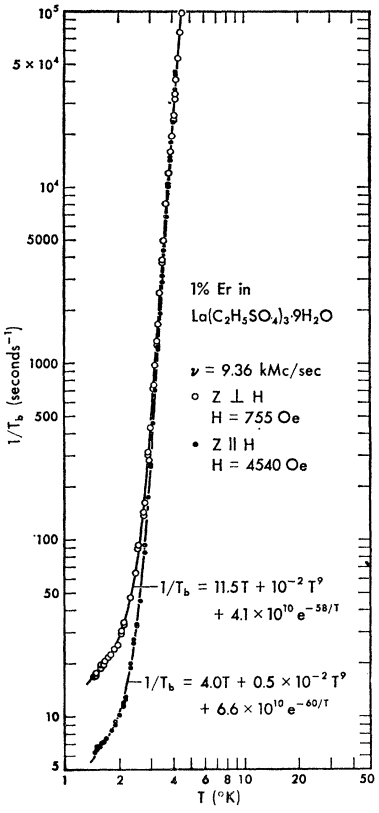


FIG. 18. Relaxation rate versus $T$ for $Er^{3+}$ in LaES, showing direct, Raman, and Orbach processes.

Since there has been no optical work on this salt, there are no data on the crystal-field parameters, the splittings $\Delta_i$, and the wave functions of the excited states. We can, however, knowing $\Delta_1/hc=15.3$ cm$^{-1}$, make a reasonable estimate of the Orbach process from Eq. (12a) if we take as a typical value of the matrix element required $\Sigma|\langle a|v_n^m|c\rangle|^2\approx 7\times 10^3$ cm$^{-2}$, the average value found by S&J for a number of similar rare-earth salts. The result is

$$T_{10}^{-1}=3.1\times 10^9 \exp(-22/T) \text{ sec}^{-1}, \quad (51)$$

in satisfactory agreement with Eq. (49). The direct and Raman processes can be similarly estimated to find $T_{1d}^{-1}\leqq 2T$ sec$^{-1}$, $T_{1R}^{-1}\approx 0.2T^9$ sec$^{-1}$ which are so small compared with the Orbach process as to be unobservable in our experiment.

### H. $Er^{3+}$ in the Ethyl Sulfate

The paramagnetic resonance spectra of $Er^{3+}$ ($4f^{11}$, $^4I_{15/2}$) in LaES[43] and in YES are quite the same, consisting of one strong central line flanked by eight hyperfine lines. For $Er^{3+}$ in YES we measure $g_{\parallel}=1.50\pm 0.05$ and $g_{\perp}=8.77\pm 0.03$; in LaES the $g$ factors are $g_{\parallel}=1.47$, $g_{\perp}=8.85$.

[43] B. Bleaney and H. E. D. Scovil, Proc. Phys. Soc. (London) **A64**, 204 (1951).

We made relaxation time measurements on a crystal of 1% $Er^{3+}$ in LaES, for $z\perp\mathbf{H}$ and for $z\|\mathbf{H}$, with the results shown in Fig. 18; the data are fitted by a least-squares computer program to the expressions

$$T_b^{-1}=11.4T+1\times 10^{-2}T^9+2.9\times 10^{10} \times\exp(-57/T) \text{ sec}^{-1}, \quad (52)$$

for $z\perp H$, and

$$T_b^{-1}=4.2T+4.4\times 10^{-3}T^9+4.5\times 10^{10} \times\exp(-59/T) \text{ sec}^{-1}, \quad (53)$$

for $z\|H$; the estimated errors in the exponential are $\pm 4$°K. These expressions differ only slightly from those given in Fig. 18 which were obtained by a hand fit before the computer program was available. Measurements on a crystal of 1% $Er^{3+}$ in YES, with $z\perp H$, $\nu=9.31$ Gc/sec, $H=759$ Oe, are fitted by the expression

$$T_b^{-1}=5.9T+3\times 10^{-3}T^9+5.0\times 10^{10} \times\exp(-63/T) \text{ sec}^{-1}, \quad (54)$$

while measurements taken on a 0.1% $Er^{3+}$ in YES crystal with $z\perp H$ fit the following:

$$T_b^{-1}=4.8T+3.2\times 10^{-3}T^9+5.8\times 10^{10} \times\exp(-64.6/T) \text{ sec}^{-1}, \quad (55)$$

again showing a gratifying independence on concentration. Figure 19 shows the energy levels in concentrated ErES taken from the work of Erath[26]; note that the first excited state at $\Delta/hc=44$ cm$^{-1}$ compares closely to the values $\Delta/hc=39.6$ cm$^{-1}$ and 41.0 cm$^{-1}$ taken from Eqs. (52) and (53).

The wave functions which we calculate from Erath's work on ErES are

$$|a\rangle=0.713|-\tfrac{7}{2}\rangle-0.701|\tfrac{5}{2}\rangle, \quad (56a)$$

$$|b\rangle=0.713|\tfrac{7}{2}\rangle-0.701|-\tfrac{5}{2}\rangle, \quad (56b)$$

$$|c\rangle=0.539|-15/2\rangle+0.527|\tfrac{9}{2}\rangle-0.657|-\tfrac{3}{2}\rangle, \quad (56c)$$

$$|d\rangle=0.539|15/2\rangle+0.527|-\tfrac{9}{2}\rangle-0.657|\tfrac{3}{2}\rangle, \quad (56d)$$

$$|e\rangle=0.837|-15/2\rangle-0.420|\tfrac{9}{2}\rangle+0.350|-\tfrac{3}{2}\rangle, \quad (56e)$$

$$|f\rangle=0.837|15/2\rangle-0.420|-\tfrac{9}{2}\rangle+0.350|\tfrac{3}{2}\rangle, \quad (56f)$$

$$|i\rangle=0.701|-\tfrac{7}{2}\rangle+0.713|\tfrac{5}{2}\rangle, \quad (56g)$$

$$|j\rangle=0.701|\tfrac{7}{2}\rangle+0.713|-\tfrac{5}{2}\rangle. \quad (56h)$$

Erath finds the crystal field parameters $A_2^0\langle r^2\rangle=125.8$ cm$^{-1}$, $A_4^0\langle r^4\rangle=-81.19$ cm$^{-1}$, $A_6^0\langle r^6\rangle=-31.06$ cm$^{-1}$, and $A_6^6\langle r^6\rangle=387.19$ cm$^{-1}$. Using these parameters we calculate, for $z\perp\mathbf{H}$, using scheme Eq. (7)

$$T_1^{-1}=4.5T+1.1\times 10^{-3}T^9+9.2\times 10^{10} \times\exp(-63/T) \text{ sec}^{-1}. \quad (57a)$$

For $z\|\mathbf{H}$, the direct process is changed to

$$T_{1d}^{-1}=9.4T \text{ sec}^{-1}. \quad (57b)$$

This agrees reasonably well with the experimental

results for the YES host lattice. Scheme Eq. (8) yields, for $z\perp H$,

$$T_1^{-1}=0.26T+7.6\times10^{-6}T^9+3.54\times10^9\times\exp(-63/T)\ \text{sec}^{-1}. \quad (58a)$$

For $z\|\mathbf{H}$, the direct process is changed to

$$T_{1d}^{-1}=0.15T\ \text{sec}^{-1}. \quad (58b)$$

### I. $Tb^{3+}$ in YES

The energy level scheme of $Tb^{3+}$ ($4f^8,{}^7F_6$) in concentrated TbES[23] is shown in Fig. 20, assuming a nuclear spin of zero. The paramagnetic resonance of this non-Kramers ion was first studied in YES by Baker and Bleaney[44] who found the lowest levels to be two singlets $|a\rangle$ and $|b\rangle$ with a spacing $\sim0.4$ cm$^{-1}$. Since the only stable isotope $Tb^{159}$ has a spin of $I=\frac{3}{2}$, there are, in fact, two zero field lines observed in Tb:YES at 12.018 and 14.932 Gc/sec, for the $m_I=\pm\frac{1}{2}$ and $m_I=\pm\frac{3}{2}$ transitions, respectively. These are shown in Fig. 21; when a magnetic field is applied with $z\|H$ one observes the four lines indicated for a microwave frequency of $\nu=17.00$ Gc/sec. The effective spin Hamiltonian[32] is

$$\mathcal{H}=g\beta HS_z+\Delta_xS_x+\Delta_yS_y+AS_zI_z, \quad (59)$$

with $S=\frac{1}{2}$, $I=\frac{3}{2}$, $g_{11}=17.72$, and $\Delta_0/hc=0.387$ cm$^{-1}$, where $\Delta_0^2=\Delta_x^2+\Delta_y^2$.

We made relaxation measurements on a crystal of 1% $Tb^{3+}$ in YES in zero magnetic field, with the results shown in Fig. 22. The relaxation data for both lines fit the expression

$$T_b^{-1}=30T+1\times10^{-2}T^7\ \text{sec}^{-1}, \quad (60)$$

indicating a direct and a Raman process. As expected from the optical measurements[23] of the ${}^6F_6$ level crystal-field splittings in Fig. 20, the level at $\Delta/hc=100.9$ cm$^{-1}$ is too high to contribute to an Orbach process. For the same crystal, data were taken at 17.00 Gc/sec with $z\|H$ for the $m_I=-\frac{1}{2}$ and $m_I=-\frac{3}{2}$ lines with the results of Fig. 23, which are fitted to the expressions

$$T_1^{-1}=95T+1.14\times10^{-2}T^7, \quad (61)$$

for the $m_I=-\frac{3}{2}$ line at 980 Oe; and

$$T_1^{-1}=59T+0.92\times10^{-2}T^7, \quad (62)$$

for the $m_I=-\frac{1}{2}$ line at 630 Oe.

From the optically measured splittings given in Fig. 20 and the crystal-field parameters taken from Fig. 2, $A_2{}^0\langle r^2\rangle=110$ cm$^{-1}$, $A_4{}^0\langle r^4\rangle=-75$ cm$^{-1}$, $A_6{}^0\langle r^6\rangle=-34$ cm$^{-1}$, and $A_6{}^6\langle r^6\rangle=465$ cm$^{-1}$, we are able to construct the following wave functions diagonal in the crystal field and spin orbit interactions.

[44] J. M. Baker and B. Bleaney, Proc. Phys. Soc. (London) A68, 257 (1955).

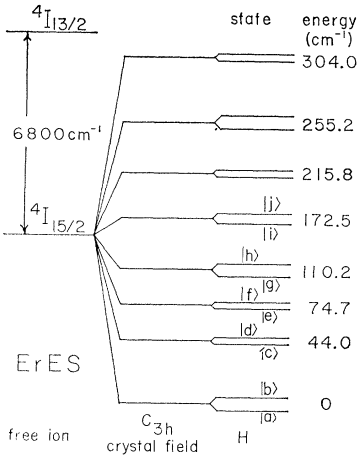


FIG. 19. Energy levels of concentrated ErES showing the crystal field splitting of the $^4I_{15/2}$ ground state, as measured by Erath (Ref. 26).

$$|a\rangle=0.707(|6\rangle+|-6\rangle)\cos\delta+\sin\delta|0\rangle, \quad (63a)$$

$$|b\rangle=0.707(|6\rangle-|-6\rangle), \quad (63b)$$

$$|c\rangle=0.910|-5\rangle+0.416|1\rangle, \quad (63c)$$

$$|d\rangle=0.910|5\rangle+0.416|-1\rangle, \quad (63d)$$

$$|e\rangle=0.062(|6\rangle+|-6\rangle)-0.996|0\rangle, \quad (63e)$$

with $\cos\delta=0.996$ and $\sin\delta=0.087$. Now the Hamiltonian we must consider is given by

$$\mathcal{H}_0=\mathcal{H}_{so}+\mathcal{H}_c+(\Lambda\beta H+aI_z)J_z+(1/2)a(I_+J_-+I_-J_+), \quad (64)$$

where the zero-order states Eq. (63) have been chosen to be diagonal for only the first two terms in Eq. (64). Since the last term in Eq. (64) involves forbidden transitions we neglect it. Only the third term in $J_z$, which is comparable to $\Delta_0$, must be considered further in its effect on the wave functions. All the states are already diagonal in $J_z$ except $|a\rangle$ and $|b\rangle$, and they can be replaced by diagonal combinations

$$|A\rangle=\cos\theta|a\rangle-\sin\theta|b\rangle, \quad (65a)$$

$$|B\rangle=\sin\theta|a\rangle+\cos\theta|b\rangle, \quad (65b)$$

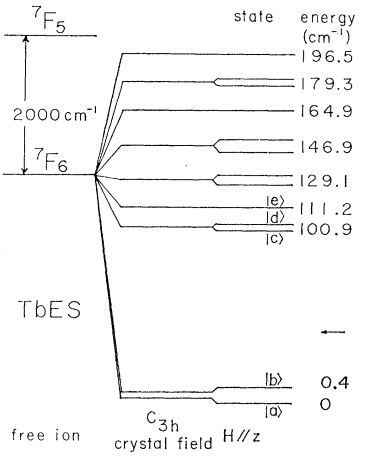


FIG. 20. Energy levels of concentrated TbES showing the crystal field splitting of the $^6F_6$ ground state, as taken from Hüfner (Ref. 23).

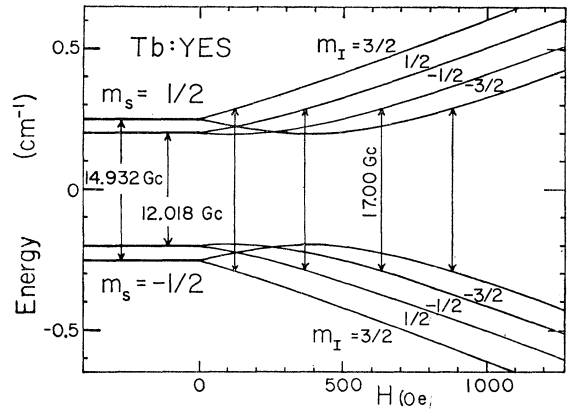


FIG. 21. Energy levels with $z\|H$ of the ground doublet as a function of magnetic field $H$ for $Tb^{3+}$ in YES, including the effect of the nuclear spin $I=\frac{3}{2}$. Baker and Bleaney (Ref. 32) give the energy levels as $E=\pm\frac{1}{2}[(g_{\|}\beta H\cos\theta+Am_I)^2+\Delta_0^2]^{1/2}$, where in our case $\theta=0°$, $g_{\|}=17.72$, $\Delta_0=0.387$ cm$^{-1}$, and $A=0.209$ cm$^{-1}$.

where $\tan 2\theta=12(\Delta\beta H+aI_z)\cos\delta/\Delta_0$. The transitions will be given by

$$h\nu=\Delta_0(1+\tan^2 2\theta)^{1/2}. \tag{66}$$

Direct calculation and evaluation of relaxation matrix elements using scheme Eq. (7) and crystal field parameters from Fig. 2, yields

$$\sum_{nm}|\langle A|v_n{}^m|B\rangle|^2=0.247+1.83\sin^2\theta\cos^2\theta. \tag{67}$$

By using Eq. (66) this can be rewritten as

$$\sum_{nm}|\langle A|v_n{}^m|B\rangle|^2=\frac{0.700(h\nu)^2-0.458(\Delta_0)^2}{(h\nu)^2}. \tag{68}$$

Using this expression in Eq. (10b) we find that the direct process will be of the general form

$$\frac{1}{T_{1d}}=(K\nu^2-K'\Delta_0^2)T. \tag{69}$$

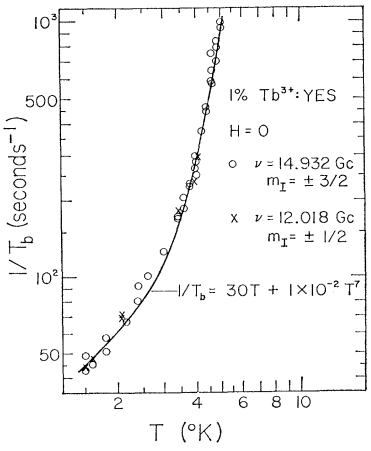


FIG. 22. Relaxation rate versus $T$ of $Tb^{3+}$ in YES for the two zero field lines at 14.932 and 12.018 Gc/sec, showing a direct and a Raman process.

Evaluation of this, as well as the Raman process, Eq. (13), yields

$$T_1{}^{-1}=17.4T+8.93\times10^{-3}T^7\ \text{sec}^{-1}, \tag{70a}$$

for $\nu=12.018$ Gc/sec; and

$$T_1{}^{-1}=37.0T+6.08\times10^{-3}T^7\ \text{sec}^{-1}, \tag{70b}$$

for $\nu=14.932$ Gc/sec. At 17.00 Gc/sec we calculate

$$T_1{}^{-1}=67.4T+4.8\times10^{-3}T^7\ \text{sec}^{-1}. \tag{70c}$$

Although the magnitudes of the observed direct and Raman processes in Figs. 22 and 23 are in good agreement with Eqs. (70a), (70b), (70c), the frequency dependence is not correctly explained. Equation (69) predicts that $T_{1d}{}^{-1}$ depends only on the frequency $\nu$; our results in Fig. 23 show that it depends somewhat on the magnetic field $H$, and in Fig. 22 for $H=0$ we find $T_{1d}$ is independent of frequency. Estimates of higher order effects [i.e., admixtures with state $|e\rangle$; and effects of the last term in Eq. (64); and slight misalignment of the crystal] are too small to explain this discrepancy. Actually the discrepancy is rather small and probably is due to cross relaxation effects. Although the direct process is strong, estimates of D in Eq. (29) shows that $DT^2\gg AT$, so that we would not expect a phonon bottleneck.

## V. SUMMARY AND CONCLUSIONS

Table II collects all the data and theoretical estimates from Sec. IV so that comparisons can be readily made. We assume that, except for the case of Pr in the ethyl sulfate which is bottlenecked, all the measured spin-bath relaxation rates $T_b{}^{-1}$ represent the true spin-lattice relaxation rate $T_1{}^{-1}$, except possibly Tb:YES. The table shows that the observed temperature behavior of the direct, Orbach, and Raman processes all have the expected theoretical dependence. In three cases (Nd:YES; Sm:LaES; Er:YES) we made variations in paramagnetic ion concentration in the range 0.1 to 1% without effect on the relaxation time; this is just

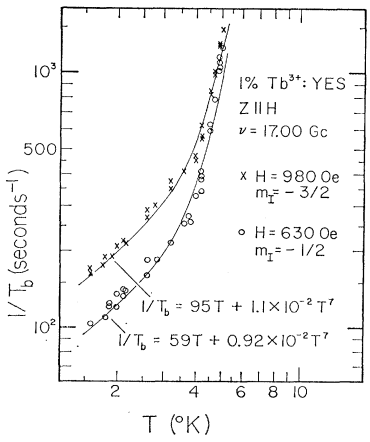


FIG. 23. Relaxation rate versus $T$ of $Tb^{3+}$ in YES for the $m_I=-\frac{3}{2}$ and the $m_I=-\frac{1}{2}$ transitions observed at 17.00 Gc/sec, showing direct and Raman processes.

TABLE II. Comparisons of measured values and theoretical estimates of the spin-lattice relaxation rates for some rare-earth ions in single crystals of the double nitrate $La_2Mg_3(NO_3)_{12}\cdot 24H_2O$ ("LaMN"), and the ethyl sulfates $La(C_2H_5SO_4)_3\cdot 9H_2O$ ("LaES") and $Y(C_2H_5SO_4)_3\cdot 9H_2O$ ("YES") in the temperature range $1.2°<T<5°K$.

| Salt | | Direct process $T_{1d}^{-1}$ (sec$^{-1}$) | Orbach process $T_{1o}^{-1}$ (sec$^{-1}$) | Raman process $T_{1R}^{-1}$ (sec$^{-1}$) |
|---|---|---|---|---|
| 2% Ce:YES | meas., Eq. (15) | | $5.1\times10^{8}\exp(-25/T)$ | $1.0T^{9}$ |
| $\angle=65°$ | theory, Eq. (22a) | $0.048T$ | $4.1\times10^{8}\exp(-25/T)$ | $1.8\times10^{-4}T^{9}$ |
| $H=4220$ Oe | theory, Eq. (22b) | $3.39T$ | $3.2\times10^{10}\exp(-25/T)$ | $1.0T^{9}$ |
| 5% Pr:LaES | meas., Eq. (24)[a] | $>5\times10^{4}T$ | $6.5\times10^{7}\exp(-21/T)$ | $(30T^{7})$ |
| $z\|\|H$ | theory, Eq. (28) | $3.6\times10^{4}T$ | $5.9\times10^{7}\exp(-20/T)$ | $6.2\times10^{-3}T^{7}$ |
| $J=2394$ Oe | theory, Eq. (27) | $5\times10^{5}T$ | $4.2\times10^{9}\exp(-20/T)$ | $1.7T^{7}$ |
| 5% Pr:YES | meas., Eq. (25)[a] | $>5\times10^{4}T$ | $3.8\times10^{7}\exp(-19/T)$ | $(30T^{7})$ |
| $z\|\|H$ | theory, Eq. (28) | $3.6\times10^{4}T$ | $5.9\times10^{7}\exp(-20/T)$ | $6.2\times10^{-3}T^{7}$ |
| $H=7010$ Oe | theory, Eq. (27) | $5\times10^{5}T$ | $4.2\times10^{9}\exp(-20/T)$ | $1.7T^{7}$ |
| 0.1% and 1% Nd:YES | meas., Eq. (31) | $1.2T$ | | $1.64\times10^{-4}T^{9}$ |
| $z\perp H$ | theory, Eq. (34) | $0.24T$ | | $3.3\times10^{-6}T^{9}$ |
| $H=3240$ Oe | theory, Eq. (33) | $0.74T$ | | $3.4\times10^{-5}T^{9}$ |
| ~1% Sm:LaMN | meas., Eq. (37) | $3.4T$ | $1.6\times10^{10}\exp(-55/T)$ | $1.3\times10^{-2}T^{9}$ |
| $z\|\|H$, $H=9150$ Oe | theory, Eq. (40) | $3.4T$ | $4.4\times10^{10}\exp(-55/T)$ | $1.5\times10^{-3}T^{9}$ |
| 0.1% and 1% Sm:LaES | meas., Eq. (41) | $1.0T$ | $5.8\times10^{8}\exp(-46/T)+6.1\times10^{10}\exp(-72/T)$ | $3.1\times10^{-3}T^{9}$ |
| $z\|\|H$, $H=11\,240$ Oe | theory, Eq. (43) | | $1.5\times10^{9}\exp(-46/T)+3.1\times10^{9}\exp(-72/T)$ | $0.89\times10^{-5}T^{9}$ |
| | theory, Eq. (44) | | $1.8\times10^{10}\exp(-46/T)+5.4\times10^{10}\exp(-72/T)$ | $3.7\times10^{-4}T^{9}$ |
| | theory, (Ref. 41) | $0.29T$ | | |
| 1% Sm:LaES | meas., (Fig. 13) | $3.3T$ | $5.8\times10^{8}\exp(-46/T)+6.1\times10^{10}\exp(-72/T)$ | $3.1\times10^{-3}T^{9}$ |
| $z\perp H$, $H=11\,100$ Oe | theory, Eq. (43) | $0.69T$ | $1.5\times10^{9}\exp(-46/T)+3.1\times10^{9}\exp(-72/T)$ | $0.89\times10^{-5}T^{9}$ |
| | theory, Eq. (44) | $6.1T$ | $1.8\times10^{10}\exp(-46/T)+5.4\times10^{10}\exp(-72/T)$ | $3.7\times10^{-4}T^{9}$ |
| | theory (Ref. 41) | $0.16T$ | | |
| 1% Sm:YES | meas., Eq. (46) | $1.3T$ | $8.0\times10^{8}\exp(-51/T)$ | $4.0\times10^{-4}T^{9}$ |
| $z\perp H$ | theory, Eq. (47a) | $0.56T$ | $3.7\times10^{9}\exp(-51/T)$ | $1.3\times10^{-6}T^{9}$ |
| $H=11\,100$ Oe | theory, Eq. (47b) | $5.0T$ | $2.4\times10^{10}\exp(-51/T)$ | $8.4\times10^{-4}T^{9}$ |
| SmES $z\|\|H$, $H=11\,015$ Oe | meas., Eq. (48) | | $9.5\times10^{8}\exp(-51/T)$ | $5.8\times10^{-4}T^{9}$ |
| ~1% Dy:LaMN | meas., Eq. (49) | | $7.0\times10^{9}\exp(-22/T)$ | |
| $z\|\|H$, $H=1558$ Oe | theory, Eq. (51) | $<2T$ | $3.1\times10^{9}\exp(-22/T)$ | $\sim0.2T^{9}$ |
| 1% Er:LaES | meas., Eq. (53) | $4.2T$ | $4.5\times10^{10}\exp(-59/T)$ | $4.4\times10^{-3}T^{9}$ |
| $z\|\|H$ | theory, Eq. (58b)[b] | $0.15T$ | $2.7\times10^{9}\exp(-58/T)$ | $1.1\times10^{-5}T^{9}$ |
| $H=4540$ Oe | theory, Eq. (57b)[b] | $9.4T$ | $7.1\times10^{10}\exp(-58/T)$ | $1.5\times10^{-3}T^{9}$ |
| 1% Er:LaES | meas., Eq. (52) | $11.4T$ | $2.9\times10^{10}\exp(-57/T)$ | $1.0\times10^{-2}T^{9}$ |
| $z\perp H$ | theory, Eq. (58a)[c] | $0.31T$ | $2.7\times10^{9}\exp(-58/T)$ | $1.1\times10^{-5}T^{9}$ |
| $H=755$ Oe | theory, Eq. (57a)[c] | $5.4T$ | $7.1\times10^{10}\exp(-58/T)$ | $1.5\times10^{-3}T^{9}$ |
| 0.1% and 1% Er:YES | meas., Eq. (54) | $5.9T$ | $5.0\times10^{10}\exp(-63/T)$ | $3.0\times10^{-3}T^{9}$ |
| $z\perp H$ | theory, Eq. (58a) | $0.26T$ | $3.5\times10^{9}\exp(-63/T)$ | $7.6\times10^{-6}T^{9}$ |
| $H=759$ Oe | theory, Eq. (57a) | $4.5T$ | $9.2\times10^{10}\exp(-63/T)$ | $1.1\times10^{-3}T^{9}$ |
| 1% Tb:YES, $z\|\|H$ | | | | |
| $H=0$, $\nu=12.0$ and 14.9 Gc/sec | meas., Eq. (60) | $30T$ | | $1\times10^{-2}T^{7}$ |
| $\nu=12.0$ Gc/sec | theory, Eq. (70a) | $17.4T$ | | $8.9\times10^{-3}T^{7}$ |
| $\nu=14.9$ Gc/sec | theory, Eq. (70b) | $37.0T$ | | $6.1\times10^{-3}T^{7}$ |
| $H=980$ Oe, $\nu=17.0$ Gc/sec | meas., Eq. (61) | $95T$ | | $1.1\times10^{-2}T^{7}$ |
| $H=630$ Oe, $\nu=17.0$ Gc/sec | meas., Eq. (62) | $59T$ | | $0.92\times10^{-2}T^{7}$ |
| $\nu=17.0$ Gc/sec | theory, Eq. (70c) | $67.4T$ | | $4.8\times10^{-3}T^{7}$ |

[a] Since the direct process is bottlenecked, only a lower limit can be obtained from Eqs. (24) and (25) by assuming $AT\gg DT^{9}$. The data fit equally well either the Orbach or the Raman process shown.
[b] The Orbach and Raman processes are obtained from Eqs. (57a) and (58a) by adjustment to the observed value of $\Delta=58°K$.
[c] All the processes are obtained from Eqs. (57a) and (57b) by adjustment to a value of $\Delta=58°K$.

what is expected for the Van Vleck-Kronig-Fierz mechanism.[13,14,15a]

Table II shows the theoretical calculations for two schemes for estimating the dynamic crystal-field parameters from the measured static parameters. For each case the first theoretical estimate listed is based on Eq. (8), and the second on Eq. (7). It is seen that, for most cases, the latter scheme gives a better agreement with the data than the first. S&J also found that scheme Eq. (7) explained their data, which was predominantly for the double nitrates. However, it is worth noting that for Ce, Sm, and possibly Pr in the ethyl sulfates, scheme Eq. (8) gives a better fit to the data for the Orbach process, whereas scheme Eq. (7) overestimates this process by one or two orders of magnitude.

We have used another simple scheme to make theoretical estimates in which we first use Eqs. (8a) and (8b) to estimate the $a_n{}^m$ parameters, and then multiply each parameter by the factor $n+1$ before using it to calculate the matrix elements $|\langle a|v_n{}^m|b\rangle|$. The factor $n+1$ arises if one makes a Taylor's expansion of the crystal field in ligand coordinates, assuming a point charge model. Huang[10] has used this same scheme and finds that it gives a reasonable explanation of his data. We have made calculations for the cases in Table II using this third scheme and find that the results do not differ much from scheme Eq. (7), except in those few cases where the matrix elements of $v_6{}^6$, $v_4{}^3$, and $v_6{}^3$ dominate.

In only two cases, Pr in the ethyl sulfate and concentrated SmES, was a phononbottleneck $T_b{}^{-1}\propto T^2$ observed. For these cases it is expected, and for the other cases it is not expected.

Although there is a small discrepancy in the frequency dependence of Tb:YES, the over-all conclusion is that theory and experiment are in reasonably satisfactory agreement for the ions of Table II. The agreement is considerably better than an order of magnitude for the direct and Orbach processes; the calculations sometimes underestimate the Raman process by an order of magnitude. In several cases [Dy:LaMN; Ce:YES; Sm:LaMN; Sm:LaES; Sm:YES] the measured Orbach relaxation process provides a determination of a previously unknown crystal field splitting $\Delta$. In some of these cases we have shown that the value of $\Delta$ in the dilute salt may differ significantly from the concentrated salt.

## ACKNOWLEDGMENTS

We wish to acknowledge with much thanks many helpful discussions with Dr. J. M. Baker. Thanks are also due to Dr. P. L. Scott, Manfred B. Schulz, and James R. McColl for assistance on various phases of this work. We wish to thank Professor H. J. Stapleton and R. C. Mikkelson for the use of their computer program on which our calculations are based.

# Errata

**Relation Between Electrons and Holes in Atomic Configurations,** GULZARI L. MALLI [Phys. Rev. **135**, A978 (1964)]. In the second term of Eq. (1) on p. A978,

$$\sum_{k=0}^{2(l_i,l_j)<} \text{ should be replaced by } \sum_k.$$

Similarly in Eq. (8), (10), and (12) on p. A979,

$$\sum_{k\neq 0}^{2(l_i,l_j)<} \text{ should be replaced by } \sum_{k\neq 0}.$$

In footnote 2, p. A978, the relation $b^k=b^kD_k'$ should read $b_k=b^kD_k'$. Equation (13), p. A979, the coefficient of $F^2(pp)$ should be 2/5 instead of 2/25.

**Tunneling into Dirty Superconductors Near their Upper Critical Fields,** E. GUYON, A. MARTINET, J. MATRICON, AND P. PINCUS [Phys. Rev. **138**, A746 (1965)]. Unfortunately, several errors in dimensions appear in the text. The corrected equations appear below:

$$\frac{N(r,\omega)}{N(0)}=1+2\frac{|\Delta(r)|^2\tau^2}{\hbar^2}\frac{[(2\omega\tau)^2-1]}{[(2\omega\tau)^2+1]^2}, \qquad \text{(I.1)}$$

$$\psi=\left(\frac{\pi}{8}\frac{m\sigma}{k_BT\hbar e^2}\right)^{1/2}\Delta, \qquad \text{(II.8)}$$

$$-\frac{1}{4\pi}\int h_s{}^2d\mathbf{r} \quad \text{instead of} \quad -\frac{1}{4\pi}\int h_sd\mathbf{r}, \qquad \text{(II.13)}$$

and consequently the last part of (II.21) becomes

$$\ldots -4\pi\left(\frac{e\hbar}{mc}\right)^2\int|\psi|^4d\mathbf{r}=0,$$

$$|\Delta_K(0)|^2=\frac{0.84}{\pi^2}\frac{ec}{\sigma}\frac{(H_{c3}-H)}{(\kappa_2{}^2-0.174)}k_BT, \qquad \text{(II.20)}$$

$$|\Delta(0)|^2=\frac{0.8}{\pi^2}\frac{ec}{\sigma}\frac{(H_{c2}-H)}{(\kappa_2{}^2-0.5)}k_BT. \qquad \text{(II.22)}$$

At the top of the right-hand column of p. A750, the equation should read

$$H_{c2}=\phi_0/2\pi\tau D.$$

The actual comparisons with experiment were made with the correct formulas and consequently the discussion given in the text is not altered. The calculations of the order parameter in the text were derived on the basis of the linearized Landau-Ginsburg equations. The generalized nonlinear equations valid at all temperatures are given in K. Maki, Physics **1**, 21 (1964).